Estuarine, Coastal and Shelf Science 276 (2022) 108023

Contents lists available at ScienceDirect

Estuarine, Coastal and Shelf Science

journal homepage: www.elsevier.com/locate/ecss

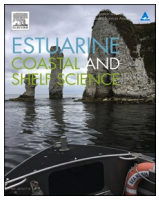

The shape and residual flow interaction of tidal oscillations

D.E. Reeve *, J.M. Horrillo-Caraballo, H. Karunarathna

Zienkiewicz Centre for Computational Engineering, Swansea University, Bay Campus, Fabian Way, Swansea, SA1 8EN, Wales, UK

ARTICLE INFO

Keywords:
Computational model
Tidal residual currents
Vorticity
Anisotropy

ABSTRACT

Tidal flows are seldom exactly sinusoidal, leading to a small discrepancy, or residual, over each tidal cycle. Although residuals are generally small in comparison with instantaneous currents, their cumulative effect is important for sediment transport and dispersion of contaminants. The meso-scale characteristics of tidal residual currents are investigated with a computational model of the Irish Sea. The role of the tidal oscillations, or eddies, in forcing the residual flow is considered first through theoretical considerations and secondly by calculating time mean flow quantities directly from the computational model. The tidal eddies contribute to the time mean vorticity balance through the tidal stresses which can be written in the form of a divergence of an eddy vorticity flux. In regions where the tidal flows are approximately horizontally non-divergent the anisotropy of the tidal eddies is strongly linked to their contribution to driving the residual flow. A measure of eddy anisotropy is proposed and this mirrors the shape and orientation of the tidal ellipses of the main tidal constituent. The vorticity balance of the residual flow is dominated by the frictional torque and the eddy vorticity flux divergence, with vorticity advection and vortex stretching by the residual flow generally being of secondary importance.

1. Introduction

An understanding of tides has proven important for optimising marine power generation and management of sediments in the coastal environment. For power generation, the energy contained in the tidal oscillation is an important metric of the available energy, (whether it be potential energy within the tidal range or kinetic energy of the tidal flow), but other factors like the symmetry of the tidal oscillation can play an important role when the practicalities of power generation are taken into account, (Neill et al., 2014). Sediment transport is a key element of coastal management, particularly where there are potential conflicts between development, conservation, tourism and aquaculture interests. The most visual impact of sediment transport is along the shoreline where beach levels and orientation can change on a daily basis in response to the action of waves. Away from the littoral zone sediment transport still takes place but is driven predominantly by large scale currents rather than waves; the currents comprising tidal and non-tidal (meteorologically-induced) parts. The non-tidal components are ephemeral and directionally inconsistent, being driven by the prevailing surface winds.

In this paper the topic of the relationship between tidal residual currents, the instantaneous tidal oscillations, irregular topography and bathymetry is explored in the context of depth-averaged meso-scale dynamics. Of particular focus is the link between the shape of the tidal oscillations and the residual currents. Tidal flows recorded at a fixed point are not generally symmetric, often having a residual non-oscillatory component. The period over which residuals are determined is an important parameter. For short term processes, e.g. aquaculture and ecology, differences in spring and neap tidal conditions can be important, as well as wind and wave interaction with tides. For longer term processes, e.g. sediment transport and decadal scale geomorphorphic changes, residuals are more usually calculated over the period of a year or more to fully capture the effects of long period tidal harmonics. Residual currents determined from tide gauge measurements are typically computed as a time average of a sequence of recordings which will contain the combined contributions from wind, wave and tidal forcing. Here, we focus on tidal residuals; those residual currents that arise solely from the interaction of tidally-forced flows with irregular topography and bathymetry. Tidal residual currents may be much smaller than instantaneous flood or ebb currents but their cumulative effects over many months or years can have significant impacts on pollutant transport and sediment movements, (e.g. McCave, 1970; Prandle, 1984; Dronkers, 1986). Correlations between long term meso-scale sediment movement and tidal residual currents have been established, (see e.g. McCave, 1970; De Swart and Zimmerman, 2009; Moore et al., 2009). The formation of gyres or circulation patterns in

* Corresponding author.
E-mail address: d.e.reeve@swansea.ac.uk (D.E. Reeve).

https://doi.org/10.1016/j.ecss.2022.108023
Received 10 September 2021; Received in revised form 3 August 2022; Accepted 8 August 2022
Available online 12 August 2022

residual currents close to headlands, and their association with sandbanks, is well-known, (see e.g. Pingree, 1978; Zimmerman, 1978). The importance of the Coriolis effect in determining the formation of sand banks and the shape of gyres near the coast has been investigated in a depth-averaged context both theoretically (Huthnance, 1973; Zimmerman, 1981; Robinson, 1983) and computationally (Pingree and Maddock, 1980; Hulscher et al., 1993; Horrillo-Caraballo and Reeve, 2008), and reproduced in more complex numerical models (e.g., Neill et al., 2007; Sanay et al., 2007).

The key physical process can be interpreted as momentum transfer from the oscillatory tidal flow to the residual flow through the nonlinear terms in the dynamical equations. As the pattern of residual currents may exhibit closed circulation cells and regions of lateral shear, this process may also be viewed as a vorticity transfer from the instantaneous tidal flow to the residual flow. From the first perspective, momentum transfer occurs through the nonlinear processes of advection and friction. If the tidal variation is viewed as a combination of tidal harmonics with distinct periods determined by equilibrium tidal theory then the nonlinear interaction may be understood in a simple way by considering the product of two cosinusoids of different frequencies:

$$U_1 \cos(\omega_1 t) \;\; x \;\; U_2 \cos(\omega_2 t) = \frac{U_1 U_2}{2}\{\cos(\omega_1 - \omega_2)t + \cos(\omega_1 + \omega_2)t\} \qquad (1)$$

where the two tidal harmonics have frequencies ω_1 and ω_2 and amplitudes U_1 and U_2 respectively. Their combination gives rise to constituents at their sum and difference frequencies courtesy of the trigonometric relationship in Equation (1). Terms involving the product of a single harmonic, sometimes referred to as 'self-interaction', generate a harmonic at twice the frequency, (an overtide), and a residual. Terms involving two distinct harmonics will create harmonics at the sum and difference frequencies, usually termed compound tides. Seabed friction is often modelled as a quadratic function of velocity, Prandle (2009), which also generates higher harmonics and residuals as illustrated by Equation (1). Visible effects of this are asymmetries in the tidal elevations, (Aubrey and Speer, 1985; Friedrichs and Aubrey, 1988; Pugh, 1996), and currents, (Dronkers, 1986; Gallo and Vinzon, 2005; Guo et al., 2019).

From the vorticity balance perspective, much attention has focussed on depth-averaged motions and the vertical component of vorticity. Prandle and Ryder (1989) compared observations with computational model results and found that depth-averaged models with suitably fine resolution can accurately simulate advective terms even in areas of complex bathymetry. Vorticity can be transferred from the tides to the residual through two mechanisms (Robinson, 1983): increased flow speed due to constriction of the flow giving rise to a greater frictional force; and the constraint of reduced water depths closer to the shore increasing the depth-averaged friction. Both mechanisms act to reinforce each other, creating gyres. Sediment located within these gyres will be transported either in suspension or as bed load around the gyre, Pingree (1978). In equilibrium, circular flow results from a balance between centripetal and pressure gradient forces. Bottom friction breaks this balance resulting in a net flow towards the centre and an accumulation of sediments being transported by the flow towards the centre of the circulation.

From both perspectives, as the predominantly linear and symmetric tide wave propagates from the deep ocean to shallow coastal waters it is modified by nonlinear interactions and topographic constraints to lose its symmetry, generating residual currents in the process. Indeed, McCave (1970) noted a correlation between the symmetry of tidal current ellipses and bedform type and geometry in the Southern North Sea, while Nihoul and Ronday (1975) demonstrated the importance of accounting for the transfer of momentum and vorticity by the tides in understanding the formation of closed circulation cells near the coast and coined the term 'tidal stresses' to denote the time mean contribution of tidal oscillations to the mean flow momentum balance. This suggests there is a link between the asymmetry in tidal oscillations, tidal stresses and residual currents which has not yet been fully articulated.

Following Nihoul and Ronday (1975) by considering the tides as 'eddies' and the residual current as the time mean flow; a Reynolds'-type flow decomposition is a natural way to analyse the dynamics. Reynolds' decomposition is more often applied to flows considered turbulent and random, (e.g. Müller, 2006), with time averages being performed over the time scales of small-scale turbulence. However, by performing averages over the period of many tidal cycles the contribution of tidal oscillations may be isolated.

We use a high resolution, nonlinear, depth-averaged barotropic model of the Irish and Celtic Sea as a tool to investigate the tidal dynamics. This region has a complicated geographical shape and intricate bathymetry. The tides are highly amplified; in some locations being classified as mega-tidal with a tidal range in excess of 8 m, (Horrillo--Caraballo et al., 2021). The model was driven by specifying conditions along open sea boundaries using a combination of 13 tidal constituents allowing compound and overtides to be generated internally by the model through the nonlinear dynamics. A long period of simulation was specified, one year, to allow accurate estimate of time averaged flow statistics arising from the multiplicity of tidal harmonic components.

The aims of this paper are twofold: first, to investigate the combination of tidal asymmetry, tidal stresses and residual currents through which new insights into the role of tidal eddies in driving residual currents may be found; and second, to interpret these ideas to three coastal sites in the Irish and Celtic Seas which have a highly energetic tidal regime. The theoretical context is discussed in Section 2. In Section 3 a brief description is given of the tidal model used in the application. Section 4 contains the results and discussions of the study and the paper finishes with a short set of conclusions in Section 5.

2. Theoretical context

The oscillatory and residual components of the flow are not independent in general. They will interact with each other with a consequent transfer of energy between the two. To understand the eddy-residual flow interaction we consider the absolute vorticity balance. This is a useful means of investigating the residual generation mechanisms. As a first, step consider the depth-averaged, Reynolds' averaged momentum equations which may be written as:

$$\frac{D\boldsymbol{u}}{Dt} + f\boldsymbol{k}\, x\, \boldsymbol{u} + \; g\nabla\eta = \boldsymbol{F} \qquad (2)$$

where $\frac{D}{Dt}$ denotes the material derivative, $\mathbf{u} = (u, v)$, is the depth-averaged velocity vector; u and v are the eastward and northward velocities, respectively; ∇ is the horizontal gradient operator; f is the Coriolis parameter; $\mathbf{k}$ is a unit vector in the vertical; ρ is the density, taken as constant; η is the displacement of the sea surface from its equilibrium position; $\boldsymbol{F}$ is the frictional acceleration consisting of bed and surface shear stresses, viscous dissipation, turbulent dissipation and vertical advection of momentum. On neglecting dissipation, vertical advection of momentum and the surface stresses the friction term simplifies to $\boldsymbol{F} = -\boldsymbol{\tau}/\rho H$, where $\boldsymbol{\tau}$ is the bed shear stress (see Eqtn 13) and H is the time varying total water depth being the sum of η, the displacement of the sea surface from its equilibrium position, and the undisturbed water depth, $h(x,y)$. The motion is considered to be in hydrostatic balance. Taking the vertical component of the curl of the momentum equation (Eq. (2)), yields the vorticity equation:

$$\frac{D\xi}{Dt} + \beta v + \zeta\nabla.\mathbf{u} = \boldsymbol{k}.\nabla x\boldsymbol{F} \qquad (3)$$

where the relative vorticity is $\xi = \frac{\partial v}{\partial x} - \frac{\partial u}{\partial y}$, the absolute vorticity $\zeta = \xi + f$, the meridional planetary vorticity gradient is $\beta = \frac{df}{dy}$, and the curl of the frictional acceleration is $\boldsymbol{k}.\nabla x\boldsymbol{F}$. Further details of the derivation of

Equations (2) and (3) are given in Appendix A. In Eq. (3) the terms are, from left to right: the generation of vorticity following the motion, which includes local generation plus vorticity advection; the change in vorticity due to the flow crossing lines of planetary vorticity; the change in vorticity due to vortex stretching or compression as the free surface varies and as the flow travels over the irregular bathymetry; the change in vorticity due to bottom friction. As f does not depend on time Equation (3) can also be written as:

$$\frac{D\zeta}{Dt} + \zeta \nabla . \mathbf{u} = \boldsymbol{k} . \nabla x \boldsymbol{F} \tag{4}$$

which expresses how absolute vorticity is conserved following the motion in the absence of friction or horizontal divergence of the flow.

Applying a time average to the vorticity equation, (Eqtn. 3), yields

$$\frac{\overline{D}}{Dt}\overline{\xi} + \beta \overline{v} + (\overline{\xi} + f)\nabla . \overline{\mathbf{u}} = \boldsymbol{k} . \nabla x \overline{\boldsymbol{F}} - \nabla . \overline{\mathbf{u}' \xi'} \tag{5}$$

where an overbar denotes a time average (over tidal cycles), a prime denotes a temporal fluctuation and $\overline{D}/Dt = \overline{u}\partial/\partial x + \overline{v}\partial/\ \partial y$. This describes how the rate of change of relative vorticity following the mean flow is controlled by the horizontal divergence of the mean flow, the time-averaged frictional acceleration and the divergence of the eddy vorticity flux where β = df/dy is the meridional gradient of planetary vorticity. The first term on the left-hand side of Equation (6) is the rate of change of vorticity following the residual flow, the second term is the change in vorticity due to the mean flow crossing lines of planetary vorticity, the third term is the change in vorticity due to vortex stretching or squeezing arising from divergence of the residual flow. The first term of the right-hand side of the equation is the vorticity production or destruction caused by the curl of the bed shear stresses and the second term is the divergence of the vorticity flux by the tidal eddies. In the limit of no horizontal divergence or frictional effects Equation (6) implies that eddies transfer vorticity to the mean flow either by changing their local curl or by altering the mean flow across contours of planetary vorticity, (the '$\beta\overline{v}'$ term). For the sake of clarity we note that we reserve the terms 'residual' to mean a time average over many tidal cycles, 'tidal eddies' to mean the departures of the instantaneous flow about the residual, and 'gyre' to refer to a circulation cell in the residual currents.

As noted by Williams et al. (2007), the divergence of the eddy vorticity flux, $\nabla . \overline{\mathbf{u}' \xi'}$, can be viewed as the curl of an acceleration in the momentum equation. Taking the time average of Equation (2) gives

$$\frac{\overline{D}\overline{\boldsymbol{u}}}{Dt} + f\boldsymbol{k}\, x\, \overline{\boldsymbol{u}} + g\nabla\overline{\eta} = \overline{\boldsymbol{F}} - \overline{\mathbf{u}' . \nabla \mathbf{u}'} \tag{6}$$

where the eddy acceleration is given by the last term on the right hand side of Equation (6). Denoting this quantity by $\boldsymbol{A}$, it may be verified that

$$\boldsymbol{k} . \nabla\, x\, \boldsymbol{A} = -\ \nabla . \overline{\mathbf{u}' \xi'} \tag{7}$$

thereby demonstrating how the eddy feedback on the mean flow via the tidal stresses is inextricably related to its impact on the vorticity of the mean flow via the eddy vorticity flux divergence.

$\boldsymbol{A}$ may also be written in terms of the divergence of the velocity correlation tensor:

$$\overline{\nabla . (\mathbf{u}' \mathbf{u}')} = \overline{\mathbf{u}' . \nabla \mathbf{u}'} + \overline{\mathbf{u}' \nabla . \mathbf{u}'} \tag{8}$$

If the eddies are approximately horizontally non-divergent then $\boldsymbol{A}$ may be taken as being equal to the divergence of the eddy velocity correlation tensor. For depth-averaged flow, the velocity correlation tensor $\mathbf{C}$ may be written as:

$$\boldsymbol{C} = \begin{pmatrix} \overline{u'^2} & \overline{u'v'} \\ \overline{u'v'} & \overline{v'^2} \end{pmatrix} = \begin{pmatrix} K & 0 \\ 0 & K \end{pmatrix} + \begin{pmatrix} M & N \\ N & -M \end{pmatrix} \tag{9}$$

where K = ½ $(\overline{u'^2 + v'^2})$ is the kinetic energy of the eddies, M = ½ $(\overline{u'^2 - v'^2})$ and N = $\overline{u'v'}$. Note that here the 'stresses' have been defined with dimensions of velocity squared as Equation (6) has been divided through by the constant density. Equation (9) demonstrates how the symmetric correlation tensor can be split into its isotropic and anisotropic components. The principal axes of $\mathbf{C}$ are at angles ½ $\tan^{-1}$(N/M) to the x-axis and the principal stresses have magnitudes K ± $\sqrt{(M^2 + N^2)}$. The principal axes define the semi-major and -minor axes of the eddies while their magnitudes are defined by the magnitude of the stresses. Two limits are evident: isotropy, where the principal axes are of the same length giving disk-like eddies; and rod-like eddies, where one principal axis has negligible magnitude. These correspond to circular and rectilinear eddy flows respectively. Between these two extremes lie elliptical disturbances, the orientation of which are determined by the angle of the principal axes, (see e.g. Simonsen and Krogstad, 2005). Assuming that the eddies are approximately horizontally non-divergent Hoskins et al. (1983) noted that the quantity

$$\alpha = \sqrt{(M^2 + N^2)}/K \tag{10}$$

Provides a non-dimensional measure of eddy anisotropy lying between 0 and 1, with the value 0 corresponding to isotropy. They also noted that, under the same assumption, the eddy vorticity flux can be written as

$$\overline{\mathbf{u}' \xi'} = \left(-\frac{\partial M}{\partial y} + \frac{\partial N}{\partial x},\ -\frac{\partial M}{\partial x} - \frac{\partial N}{\partial y} \right) \tag{11}$$

and so

$$\nabla . \overline{\mathbf{u}' \xi'} = \left(-2\frac{\partial^2 M}{\partial x \partial y} + \frac{\partial^2 N}{\partial x^2} - \frac{\partial^2 N}{\partial y^2} \right) \tag{12}$$

where further details may be found in Appendix C. This shows that the divergence of the eddy flux depends on the anisotropy of the tidal eddies. If eddies are able to drive a mean flow, thereby transferring energy from themselves to the mean flow, then it might be reasonably thought that the most energetic eddies have the greatest propensity to force the mean flow. However, Equations (11) and (12) show that the forcing of the residual flow is determined by the anisotropy of the eddies. We return to this point in Section 4.3.

Where the assumption of approximate horizontal non-divergence is not applicable the simplification above is not possible and an analysis of the divergence of the eddy vorticity flux divergence or tidal stress term in the mean vorticity and momentum equations respectively is necessary.

3. Computational model description

3.1. Study site

The study domain covers the Irish Sea and part of the Celtic Sea, (see Fig. 1). The Irish Sea is approximately 300 km long and its width varies between 75 and 200 km. At its northern end it is joined to the Atlantic Ocean via the North Channel and at its southern end to the Celtic Sea via St. George's Channel. It extends southwards from North Channel between Larne and Corsewall Point to a line joining Carnsore Point (Ireland) and St. David's Head (Wales) in the south, (Bowden, 1980), beyond which lies the Celtic Sea, which in turn meets the Atlantic Ocean at the 200 m depth contour, (Pingree, 1980). The North Channel has a width of approximately 30 km, a depth exceeding 275 m, and connects the Irish Sea to the Atlantic Ocean. The eastern region of the Irish Sea is relatively shallow with average depths of 30 m. Olbert et al. (2012) note that while the circulation within the sea is driven by tides, winds and baroclinic flow, the M_2 and S_2 tidal constituents are the greatest contributors to barotropic flow; that tidal currents in excess of 1 m/s occur near headlands and in both North Channel and St. George's Channel, while the weakest tidal currents occur in the western Irish Sea. At its northern end, the Irish Sea extends 195 km from east to west with the

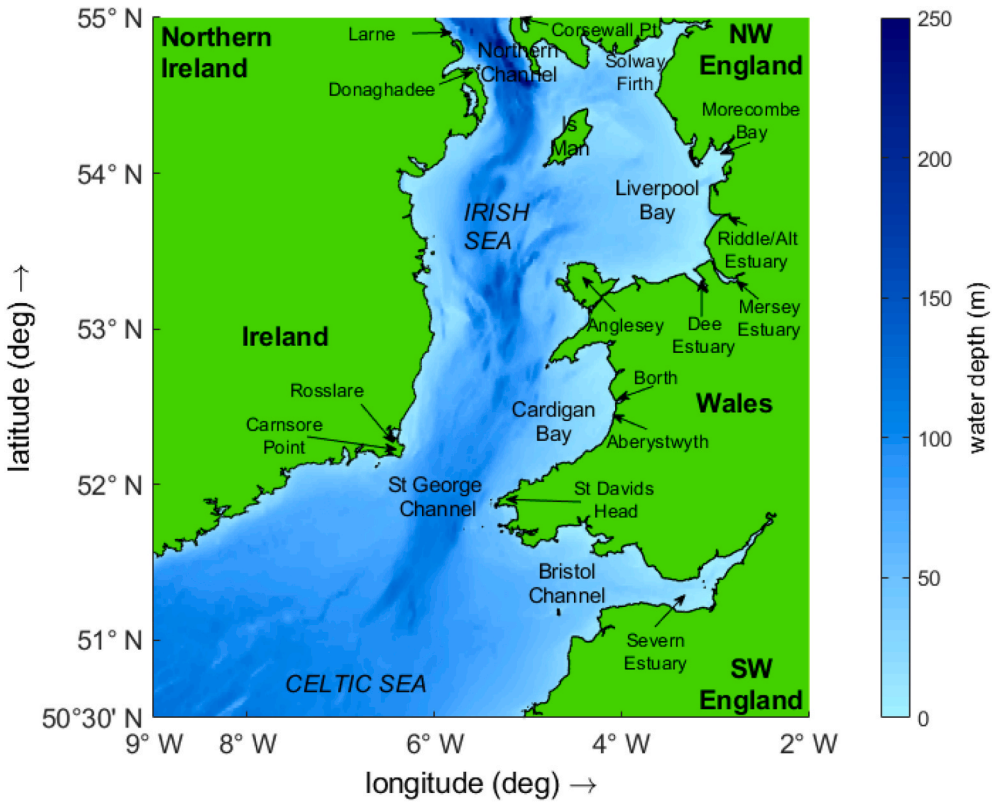

Fig. 1. Map of study area (showing bathymetry and key features of the area).

Isle of Man towards the centre. Howarth (2005) notes that extensive sandbanks can be found to the north and east of the Isle of Man (Bahama and King William Banks) and off the Irish coast south of Dublin (Kish, Codling, Arklow and Blackwater Banks).

The tides around the Welsh coast can be highly amplified, in some locations having tidal ranges above 9 m and tidal streams of 1 m/s or more, Robinson (1979). There are notable shallow areas along the Welsh coast including Liverpool Bay in the north and Cardigan Bay along the west coast. Carmarthen and Swansea Bays along the south coast have significant bedforms including Helwick, Scarweather and Nash sandbanks. There are two major estuaries, Bristol Channel/Severn Estuary lying between Wales and England in the southeast of the domain and the Solway Firth lying between Scotland and England to the north east. In addition there are numerous smaller estuaries around Liverpool Bay. These can all be strongly stratified so while the model extends part way into these estuaries to describe the tidal prism it is not intended to mimic the three dimensional flows in them.

3.2. Computational model

For this study we have used Delft3D which is an open source three-dimensional (3D) model controlled and developed by Deltares (https://oss.deltares.nl/web/delft3d). It uses finite-difference approximations to compute solutions to the 3D Navier-Stokes equations with a choice of turbulence schemes and gridding. Here, the model is configured to solve the depth-averaged flow on a sequence of nested grids, accounting for the curvature of the Earth. Details of the derivation of the equations used in Delft3D, and the computational solution methods may be found in the paper by Lesser et al. (2004). An outline derivation is included in Appendix A.

The hydrodynamic model is based on a set of two structured orthogonal curvilinear spherical grids nested to provide increased resolution in areas where the bathymetry has small scale variability. The areas covered by the two grids shown in Fig. 2.

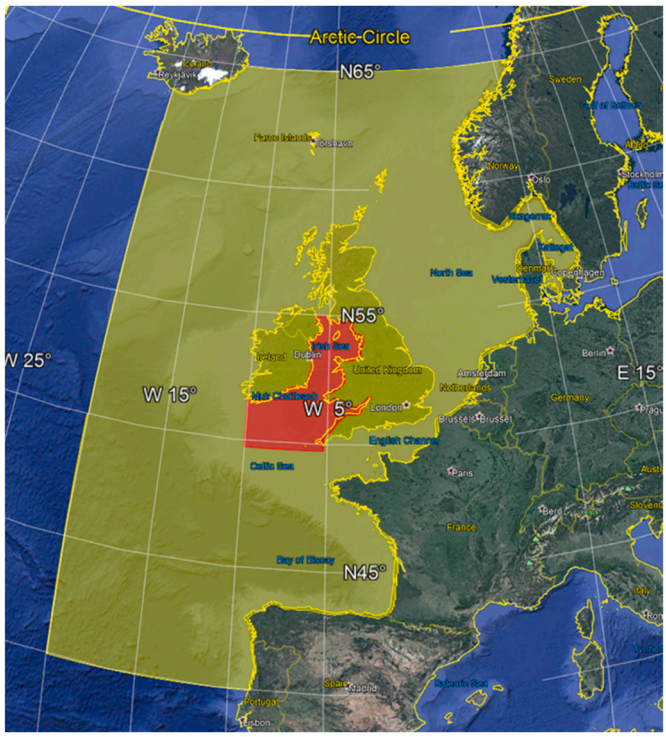

Fig. 2. Limits of the grids used for the tidal models (Continental Shelf Model, CSM – Yellow; Irish & Celtic Seas Model, ICSM – Red). Image taken from Google Earth. (For interpretation of the references to colour in this figure legend, the reader is referred to the Web version of this article.)

In the following, we refer to the Continental Shelf Model (CSM) that covers an area bounded by latitudes 40°N and 60°N and by longitudes of 20°W and 12°30′E, and the Irish and Celtic Seas Model (ICSM) that covers the area bounded by latitudes 55°N (Glenarm, Northern Ireland) and 49°30′N and by longitudes of 5°12′W (Lizard Point, UK) and 10°W. The CSM contains 590 × 506 cells and the grid spacing is approximately 3.5 km (0.03°) while the ICSM contains 416 × 304 cells and the grid spacing is less than 2 km (0.0167°). The boundaries of the CSM were chosen to extend beyond the continental shelf. Garrett & Greenberg (1977) indicated that coastal tidal models should generally extend to the edge of the continental shelf. We have extended our model beyond the shelf so that the model generates shoaling, reflection and shallow water tidal harmonics at the model grid resolution, rather than being specified at the boundaries at the coarser TPX08 resolution. The ICSM covers the Welsh coastal waters.

The bathymetries for the CSM and the ICSM have been derived from the datasets of: ETOPO, (Amante and Eakins, 2009); the GEBCO 2014 30 arc-second bathymetry, (see Weatherall et al., 2015); and EMODNET, (EMODNET, 2016). They have been integrated and interpolated onto the model grids converting all levels relative to Mean Sea Level (MSL).

A free surface condition was applied to the upper boundary and the bottom boundary was set to be an impermeable bed with a quadratic friction law. Specifically, the bed shear stress for the 2D depth averaged flow is given as follows, (Lesser et al., 2004):

$$\tau_b = \frac{\rho_0 g \mathbf{u}|\boldsymbol{u}|}{C_{2D}^2} \tag{13a}$$

where $|\mathbf{u}|$ is the magnitude of the depth-averaged horizontal velocity. The denominator C_{2D}^2, is the square of the 2D-Chézy coefficient C_{2D} [$m^{1/2}s^{-1}$]. Eddy dispersion coefficients accounting for turbulent stresses and vertical momentum transfer were set to zero.

Open boundary conditions for the CSM were specified as time-varying surface elevations determined from the TPXO8.0 OSU Tidal Inversion Software, (OTIS - from Oregon State University, https://www.tpxo.net/global/tpxo8-atlas, based on Egbert and Erofeeva, 2002), considering the 13 tidal constituents: M_2, S_2, N_2, K_2, K_1, O_1, P_1, Q_1, MF, MM, M_4, MS_4 and MN_4. Boundary conditions for the ICSM were derived directly from the results of the CSM, interpolating along the boundaries of the ICSM. For both models a 5-day spin-up period was allowed prior to creating a one year simulation.

3.3. Model calibration and validation

Initially a set of sensitivity tests were performed to check the performance of the nested models with respect to grid sizes and time step. A balance between compute time and accuracy led to the choices of ~3.5 km grid resolution for the CSM, a ~1 km grid resolution for the ICSM and a time step of 2 min in each case. The model was calibrated to determine the optimum value of the Chézy coefficient by comparison of model output against observations. Computed tidal elevations for the two month period 1st January to March 1, 2003 were compared against measured elevations at 49 coastal observation locations around the CSM domain. This information is available within the DELFT modelling suite through the DELFT Dashboard facility, (Van Ormondt et al., 2020), which contains tidal information based on observations from the International Hydrographic Organisation. Harmonic analysis was performed on sequences of tidal elevations computed in the ICSM and compared against those in the DELFT Dashboard. The amplitudes and phases of the eight major harmonics were compared with the same quantities at the 49 locations in DELFT Dashboard. The procedure was repeated for different values of the Chézy coefficient. The optimum value of the Chézy coefficient was determined to be 60 $m^{½}/s$ for the ICSM. Results using the calibrated model were validated against an independent period of data to test the calibration. Validation was undertaken over the period between 1st February 2015 and 1st February 2016. A detailed description of the calibration and validation process is presented in Horrillo-Caraballo et al. (2021). All results shown in the following sections have been derived from the validated ICSM.

3.4. Computational details

Residual currents are defined formally as the time average of the instantaneous tidal currents. For a signal composed of a single harmonic we can guarantee that an average over a whole number of wave periods will yield a result of zero. In general, with a signal comprising multiple harmonics, the average has a damped oscillatory nature as the averaging period increases. If the averaging period is sufficiently long, the contribution of the averaged oscillatory terms becomes negligible. This may be understood by considering the case where the tidal flow component follows a cosinusoidal variation in time: $u(t) = \alpha cos(\Omega t)$ where α is a constant amplitude and Ω is the period of oscillation. Integrating this function over an averaging period T, and dividing by the length of the averaging period, yields $\overline{u(t)} = \alpha sinc(\Omega T)$, where an overbar denotes a time-average and $sinc(x)$ is the '*sinc*' function, which is closely related to the spherical Bessel function of the first kind, (Bracewell, 1999). Here, we have chosen a period of one year, which is sufficient to isolate the 37 predominant harmonics, (Parker, 2007), and which is many multiples of the periods of fortnightly, diurnal, semi-diurnal and dominant shallow water harmonics.

Vorticity is a derived quantity, not computed directly within DELFT 3D, and was determined using finite difference approximations. Time sequences of vorticity at each grid point were computed from the time histories of horizontal velocity components, from which time mean and fluctuating components were determined. In a similar fashion, time histories of the bed stresses and their curl were computed at each grid point from the time histories of velocity and total water depth. Centred difference formulae were used to provide second order accuracy. The exception to this was at boundary points where one-sided formulae were used, with first order accuracy.

4. Results

In this section a detailed description of tidal properties at a regional scale is given, including tidal residual currents, statistics of the oscillatory tidal component of the flow and vorticity of the residual flow. In addition, three sites are presented in further detail: Swansea Bay, Arklow Sands/Wicklow, and the Llŷn Peninsula.

4.1. Tidal residual currents

Computed residual currents for the whole domain are shown in Fig. 3. Vectors are plotted with uniform length to aid visibility. Current speed magnitudes are shown by coloured contours. Overall, the residual currents are relatively weak in comparison to instantaneous flood and ebb currents, (<0.1 m/s), and around 0.01 m/s away from the coastlines. Previous modelling studies have shown typical tidal residual currents of 1–3 cm/s over the continental shelf around the UK, (Prandle, 1978, 1984). Residual currents are generally northward in the Irish Sea, in agreement with the observations of Bowden (1980). There is a southward flow from St. George's Channel into the Celtic Sea and northward flow along the north Devon coast. Residual flow in Cardigan Bay is generally towards the shore while the pattern in Liverpool Bay is less clear with the suggestion of gyres in the flow pattern. Detailed plots for the three selected sites are shown in Fig. 4a–c.

In Swansea Bay, (Fig. 4a), there are distinct gyres in the residual currents; a small anticlockwise one near Mumbles Head and a larger clockwise one near Porthcawl. Near the coast there is a general westward drift from the River Neath towards the Mumbles and an eastward trend from the River Neath to Porthcawl. The eastward drift is much stronger than the westward drift near the Mumbles and forms a strong

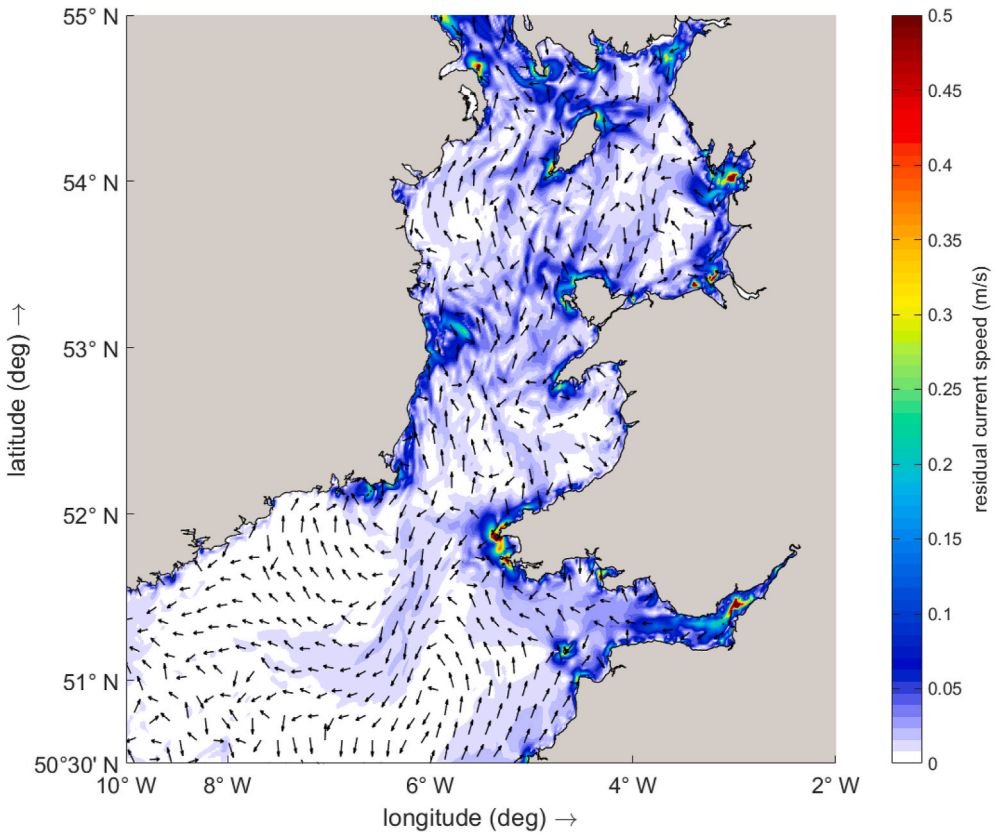

Fig. 3. Computed residual currents, (ms^{-1}). Arrows are unit length to show direction while magnitudes are shown by colour contour. (For interpretation of the references to colour in this figure legend, the reader is referred to the Web version of this article.)

offshore clockwise gyre. The gyre coincides with submerged sandbanks known as Kenfig Patches in general agreement with the arguments of sediment being captured by residual current gyres. There is qualitative agreement with the lower spatial resolution findings of Heathershaw and Hammond (1979) and Uncles (1982) regarding a clockwise circulation around Scarweather Sands to the west of Porthcawl, and with the modelling of Owen (1980) with respect to the anticlockwise nearshore flow in the northern part of the bay around The Mumbles. The downstream sense of residual currents in the Bristol Channel is in agreement with the computational results of Uncles (1982).

Near Wicklow, (Fig. 4b), convergence of residual currents from the north and south are associated with a strong offshore residual flow and a clockwise/anti-clockwise pair of gyres as might be expected from the arguments of Zimmerman (1981). The magnitude and pattern of residual currents in this zone agrees very well with those computed by Chatzirodou et al. (2017) with a depth-averaged model. This pattern of residual currents is indicative of a trend of offshore movement of material by tides into the nearby sandbank complex. The results differ from the computational results of Holt and James (2006) who presented surface residual currents in a 3D model. These show offshore directed residual flow without the convergence nearshore. Around the Llŷn Peninsula, (Fig. 4c), there appears to be an acceleration of alongshore residual flow towards the tip of the peninsula as well as the formation of a well-defined anticlockwise gyre to the south of the tip and a more diffuse clockwise gyre to the northwest. The convergence of residual currents along the north and south edges of the Llŷn peninsula, the presence of an anticlockwise gyre to the south of the tip of the peninsula and maximum residual magnitudes of approximately 0.25 m/s agree well with the findings of Neill et al. (2007). The existence of such patterns in residual currents is expected from the work of Pingree and Maddock (1979), Zimmerman (1981) and Robinson (1983) as the result of oscillatory tidal flows past a coastal headland generating vorticity in the mean flow. However, it requires a high-resolution computational approach to determine the detailed structure of residual current patterns in the realistic, non-idealised conditions considered here.

Closed circulation cells or 'gyres' in the residual currents can signify regions in which mobile sediment is trapped, (e.g. Takasugi et al., 1994; Chatzirodou et al., 2017). Robinson (1983) argued that such gyres can be understood as a transfer of vorticity from the fluctuating tidal motion to the residual flow. The importance of squeezing and stretching of the water column over the sea topography as a vorticity generation mechanism was noted by Zimmerman (1981), while Pingree and Maddock (1979), Robinson (1983) and Ridderinkhof (1989) argued that in shallower waters the torque from the bottom friction force may also be significant. These arguments can be understood by reference to Equation (6) that describes how the rate of change of absolute vorticity following the mean flow is controlled by the horizontal divergence of the mean flow (the stretching/squeezing term), the bottom friction and the divergence of the eddy vorticity flux. To understand the relative contribution of these processes towards generating the residual currents requires an investigation of the eddy dynamics and how these influence the tidal residual currents.

4.2. Eddy dynamics

From the discussion of the vorticity dynamics in Section 2 it may be anticipated that the shape, and more specifically the isotropy, of the tidal oscillations may be important. If eddies are to drive a residual flow then they must have sufficient energy themselves to transfer energy to the mean flow. One measure of the kinetic energy within the tidal oscillations is provided by the time average of $\frac{1}{2}(u'^2 + v'^2)$. This quantity is presented in Fig. 5, and shows areas of distinct concentration of tidal energy. The principal ones are the Bristol Channel/Severn Estuary, the Solway Firth, Morecambe Bay, northwest of the Isle of Man and into

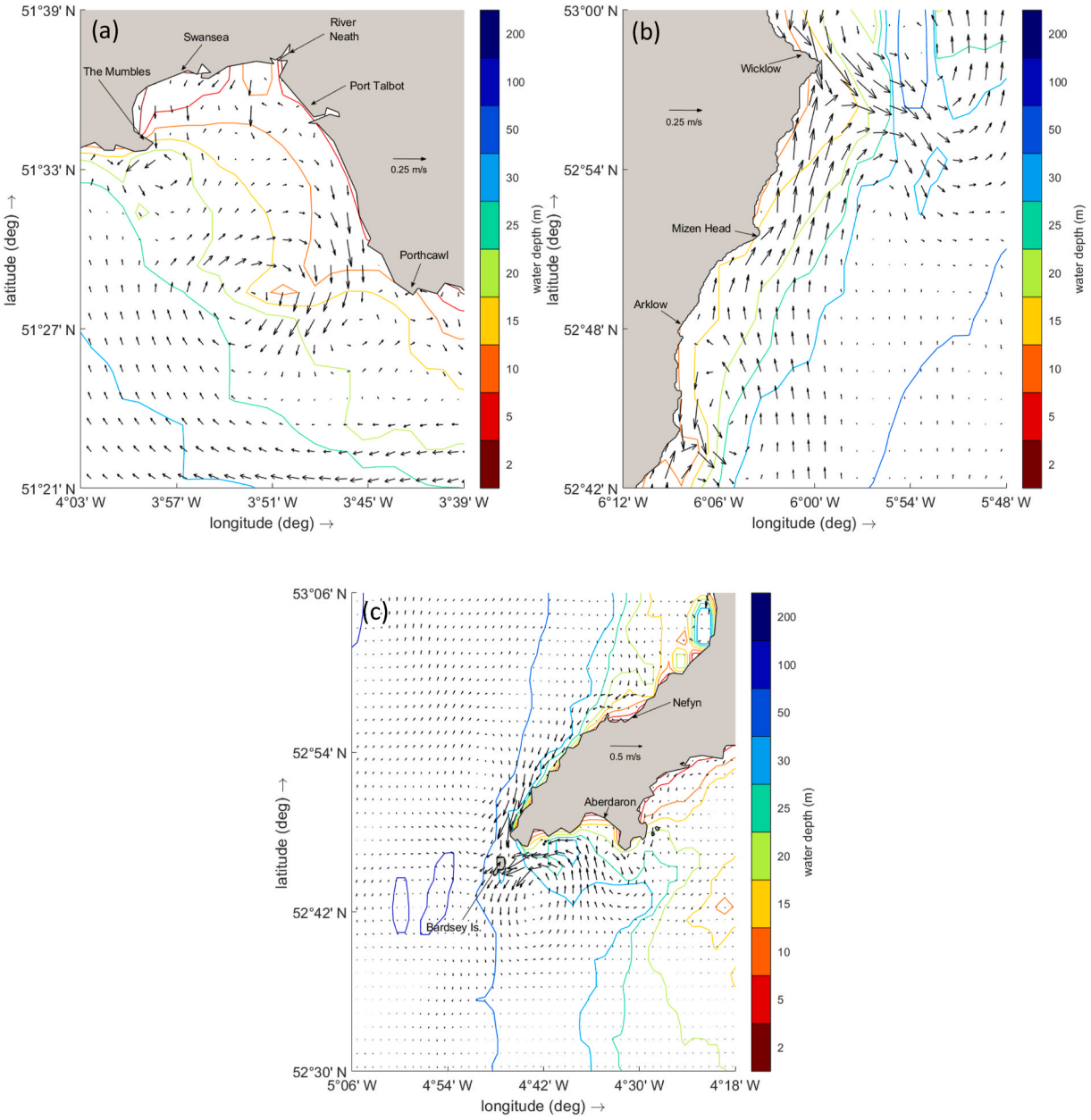

Fig. 4. Computed residual currents, (ms^{-1}), and depth contours: (a) in Swansea Bay; (b) around Arklow Sands/Wicklow; and (c) around the Llŷn Peninsula.

North Channel, northwest of Anglesey and St David's Head. The whole of St George's Channel has elevated energy caused by the constriction of flow by the narrow region between the west Welsh coast and the Irish coast around Rosslare. Notable is the relatively low energy of tidal oscillations in Cardigan Bay, outer Liverpool Bay, off the coast to the south of Donaghadee, and in the Celtic Sea in the southwest of the study domain, (highlighted areas in Fig. 6).

An alternative perspective is provided by the velocity correlation tensor. As noted in Section 2, if the tidal eddies are approximately horizontally non-divergent, it is their anisotropy that drives the mean flow. Horizontal divergence in the depth integrated flow is associated with changes in the depth of the water column, arising from variations in seabed level and tidal surface elevations. In shallow waters the tidal wave amplifies through shoaling, so a simple measure of non-divergence is given by the local ratio of half the maximum tidal range, (the maximum tidal amplitude), to the mean water depth. This quantity is shown in Fig. 6. Over a large proportion of the model domain this quantity is less than 0.1, so the assumption of approximate horizontal non-divergence would seem reasonable. The main deviations from this are in Liverpool Bay, Cardigan Bay, the Bristol Channel and to the north of Dublin Bay.

Fig. 7 shows the anisotropy factor, α, (Equation (10)), which ranges from 0 (isotropic) to 1 (strongly anisotropic). Values of 0.4, 0.6 and 0.9 correspond to a ratio of major and minor axis scales of about 3 to 2, 2 to 1 and 9 to 2 respectively.

The anisotropy of the tidal oscillation is high throughout much of the domain. There is a notable "bulls' eye" west of the outer Bristol Channel and to the southwest of the Isle of Man where the tidal oscillation becomes virtually isotropic. Other bulls' eyes occur in Cardigan Bay and to the east of the Isle of Man but these are in areas where the assumptions used in deriving the anisotropy are less valid.

Fig. 8 shows the angle of the principal axis of the velocity correlation tensor that lies between ±90° with the x-axis. The blue and red colours correspond to tidal oscillations with a NW-SE and NE-SW orientation respectively. From this we can see that the tidal eddies are elongated along a SW-NE axis in the Celtic Sea. In St. George's Channel this

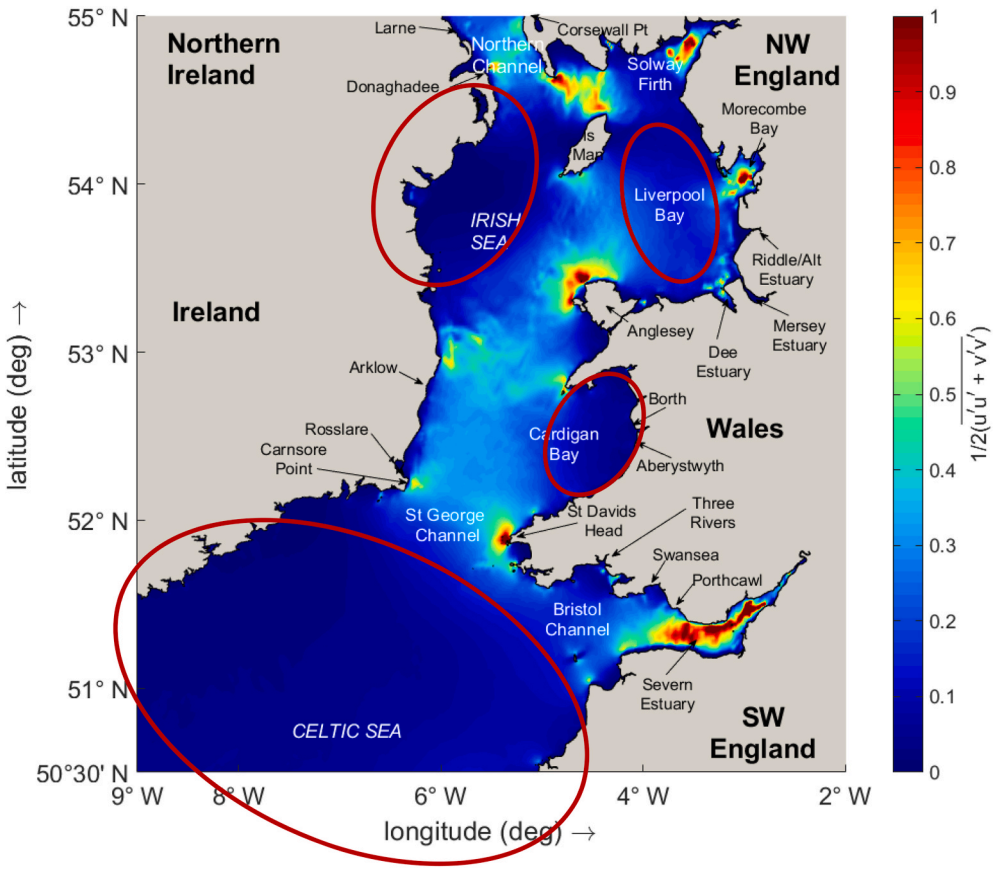

Fig. 5. Tidal eddy kinetic energy, (EKE), (m^2s^{-2}). Areas of low energy eddies are highlighted in red. (For interpretation of the references to colour in this figure legend, the reader is referred to the Web version of this article.)

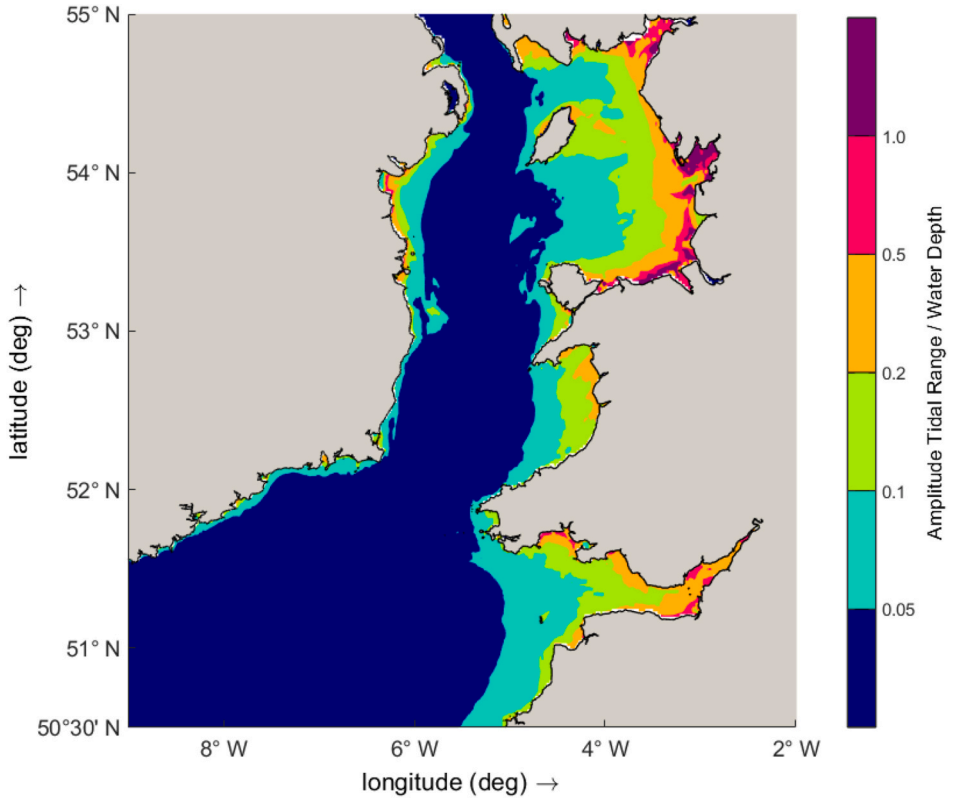

Fig. 6. The ratio of the maximum tidal amplitude to undisturbed water depth.

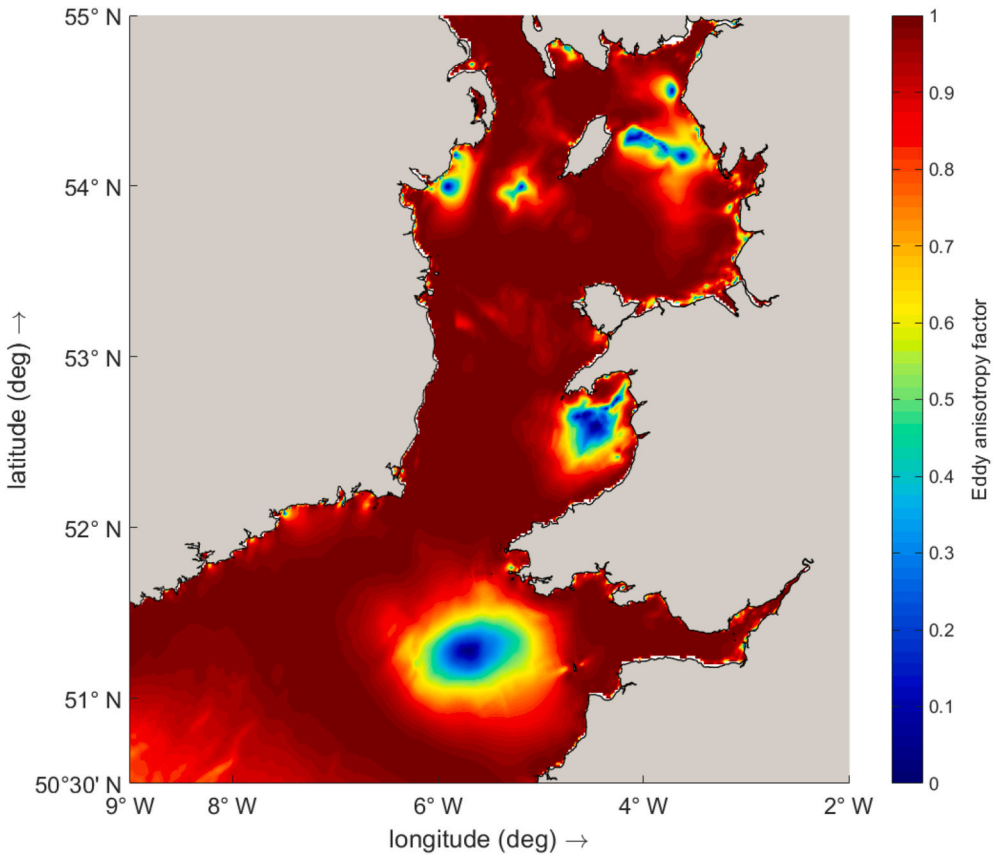

Fig. 7. Eddy anisotropy factor, (see Equation (10)).

orientation changes to be more S–N. In Liverpool Bay and the Bristol Channel the eddy orientation is close to W-E. The eddy orientation flips between SSE-NNW and SSW-NNE to the southwest of Pembrokeshire, around Wicklow and the Dublin Bay area and in the North Channel.

An interesting comparison can be made between the information held in the eddy velocity correlation tensor and tidal current ellipses. These quantities are not the same, the former being time averaged velocity fluctuations from the residual while the latter is a depiction of the tidal flow over one tidal cycle due to an individual tidal harmonic and shows the sense of rotation of the tide. Here, we choose M_2 as this is the predominant tidal harmonic, and the tidal ellipses derived from the ICSM are shown in Fig. 9.

The ellipses are colour-coded as follows: blue for clockwise and purple for anti-clockwise rotation. The semi-axes are proportional to the magnitude of the tidal currents. The rotation of the tides is predominantly clockwise along the Irish coast and anti-clockwise along the Welsh coast. Almost circular ellipses are evident in Cardigan Bay, the northern part of Liverpool Bay, an area SSW of St David's Head, and towards the southwestern corner of the domain approaching the deeper Celtic Sea. Comparing Figs. 7 and 8 with the tidal ellipses for M_2, (Fig. 9), it is easy to discern that regions of low anisotropy correspond to more circular tidal ellipses while the highly elongated ellipses occur in regions of high anisotropy, even in areas where divergence effects might be important. Also, there is a high degree of correspondence between the angle of the principal axis of the velocity correlation tensor and the orientation of the semi-major axis of the tidal ellipses. In making such a comparison it should be recalled that the ellipses are based on the contribution of the M_2 tidal constituent only while the anisotropy is calculated using the tidal flows generated by the multiplicity of tidal constituents. Nevertheless, the correspondence between the shape of the tidal ellipses and the anisotropy factor is striking and suggests, at a regional scale, they can be used interchangeably or at least as a proxy for each other. The anisotropy has the advantage of being more straightforward to compute and to plot, but gives no indication of the sense of rotation of the tidal flow.

4.3. Vorticity balance of the residual flow

4.3.1. Regional scale

The vorticity equation of the residual flow shows that a balance must be retained between advective effects, meridional motion coupled with the gradient in planetary vorticity, vortex stretching, friction effects and the divergence of the eddy vorticity flux. Fig. 10a–e shows maps of the five terms in Equation (5), from left to right. (Note the changes in scale in each plot).

A number of points are evident:

1) Vorticity generation and destruction is largely confined near to the coast, as well as in St George's Channel and North Channel;
2) The advection of planetary vorticity, the 'βv' term, is several orders of magnitude smaller than the other terms. This may be understood from the characteristic spatial scale of the flow which is several magnitudes smaller than planetary-scale oscillations such as Rossby waves for which the 'βv' term is important, (see e.g. Haltiner and Williams, 1980);
3) The primary balance is between eddy flux divergence and bed stress;
4) Advection and vortex stretching while important, have a secondary importance in terms of magnitude;
5) The distribution of vorticity generation matches the magnitude of tidal residual currents moderately well. Linear correlation coefficients computed over the whole computational domain between residual current magnitudes, (Fig. 3), and vorticity generation due to stretching, bed friction and eddy vorticity flux divergence are 0.5, 0.3 and 0.5 respectively.

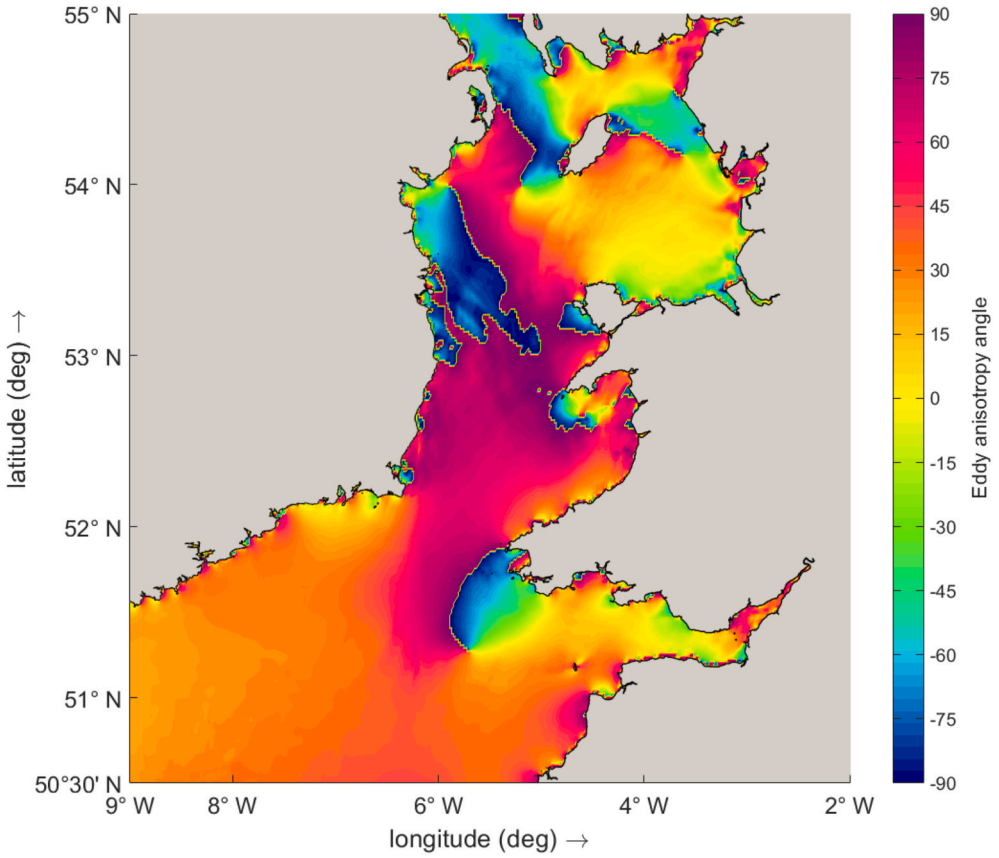

Fig. 8. Angle of the principal axis of the velocity correlation tensor lying between ±90° with the *x*-axis.

4.3.2. Local scale

A detailed picture of the vorticity balance is presented for three areas exhibiting different dynamics. The first is Swansea Bay, whose shape causes a gyre in the residual flow, and which was the site of a proposed tidal lagoon energy generation scheme. The second is Arklow Sandbanks, off the coast of Ireland, in which there are a set of offshore sandbanks, which are also home to an offshore wind turbine farm. The final area is the Llŷn Peninsula which provides a strong geographical control of the flow.

4.3.2.1. Swansea Bay. In Fig. 11a a strong clockwise gyre is located at the eastern end of Swansea Bay off the Porthcawl headland. From the shoreline, the seabed gradually deepens to a maximum of 20 m in its outer extent, but this varies due to the presence of significant sand bars, banks and submerged rocks including Scarweather Sands, Hugo Bank and Kenfig Patches. The centre of the gyre is located towards the tip of the outer shoals. A weaker, more diffuse anticlockwise gyre can be discerned to the east of this area, forming a quite unbalanced vortex pair. An anticlockwise gyre is evident off Mumbles Head at the western end of Swansea Bay. This is centred over Mixon Shoal, which is composed of mobile material so is not a fixed control on the hydrodynamics.

Fig. 11b–c shows the vortex stretching by the residual flow, the friction and the eddy flux divergence terms respectively which are the predominant in the vorticity balance of the residual flow. Neither the dipole gyre configuration off Porthcawl with a dominant clockwise gyre nor the single gyre off Mumbles Head conform with the arguments of Pingree (1978). It is clear that in these locations the primary balance is between the frictional torque and the eddy vorticity flux divergence. Stretching by the residual flow plays a secondary role and acts to reinforce the anticlockwise gyre on its seaward side and to reduce it on its shoreline flank.

4.3.2.2. Arklow Sands/Wicklow. There is a complex of sandbanks extending out from Wicklow Head which includes Arklow Sands. This could be construed as an archetypal isolated headland but with the additional effects of offshore sandbanks. These have an effect on both the tidal oscillations, evident in the energy of the eddies in this area shown in Fig. 5, and on the transfer of vorticity to the residual currents (see Fig. 10a–f). In Fig. 12a shows a clockwise gyre to south of Wicklow and anticlockwise gyre to the north. The nearshore residual currents converge on Wicklow Head and produce a strong offshore flow. We do not find the intense clockwise circulation around Arklow Sand that Chatzirodou et al. (2017) report, but in most other respects the patterns of residuals is very similar in magnitude and direction. This matches the archetypal situation more closely although the gyre pattern is modified by the flows induced by the nearby sandbanks and shoals.

The main balance is between the frictional torque and eddy vorticity flux divergence off Wicklow Head but in the region off Arklow the vortex stretching by the residual flow becomes more important.

4.3.2.3. Llŷn Peninsula. The Llŷn peninsula is at the north end of Cardigan Bay, is aligned northeast/southwest and is approximately 40 km long. At its seaward tip the seabed drops rapidly to approximately 30 m depth before rising to Bardsey Island. Fig. 13a shows the residual flow and its vorticity. Despite the complex bathymetry this system behaves similarly to other headland systems in many aspects, with a residual flow away from the tip of the headland and a dipole pattern of residual current gyres on either side of the headland. The residual gyres are not symmetric, with the anticlockwise gyre centred to the southeast of Bardsey Island lying over the large sand bank Bastram Shoal being more pronounced. There is no corresponding bank to the northwest associated with the more diffuse clockwise gyre. Further, on the northern flank of the peninsula the residual currents take the form of a jet running parallel to the coastline. This results in tongues of positive

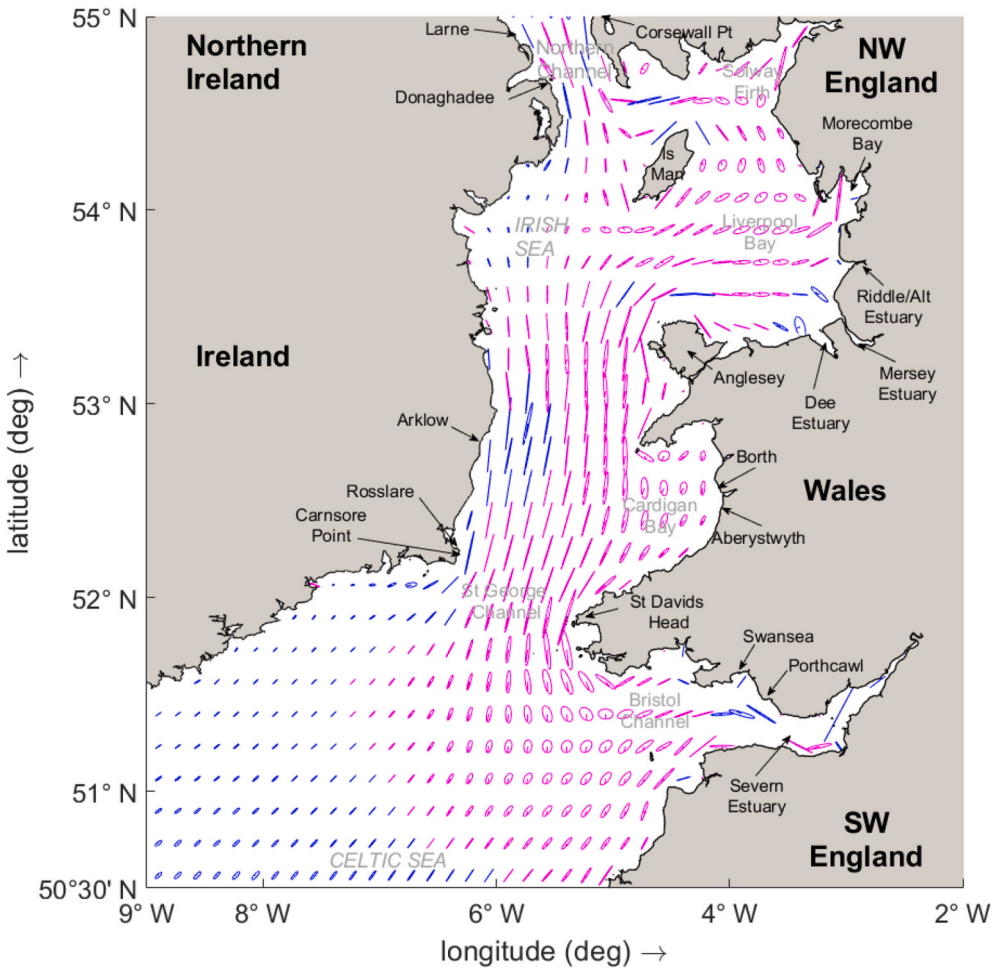

Fig. 9. Tidal ellipses of the M_2 tidal constituent shown every 10 grid points. Blue indicates clockwise rotation and purple anti-clockwise rotation of the tidal flow. (For interpretation of the references to colour in this figure legend, the reader is referred to the Web version of this article.)

and negative vorticity extending either side of the peak of the jet due to the strong shear across the jet.

From the smaller (sub) peninsula, stretching southeast from Aberdaron, a second set of dipole circulations is evident in the residual flow pattern, this time with the clockwise gyre being more prominent. The main balance is again between the eddy vorticity flux divergence and the frictional torque in the regions of the residual gyres. Along the Llŷn Peninsula the seabed shoals steeply towards the shore; thus vortex stretching is significant, together with frictional torque. The relatively large distortion of the tidal oscillations suggests that eddy vorticity flux divergence is also important. The frictional torque and eddy vorticity flux divergence terms generally act in opposition to each other around the peninsula.

5. Discussion

The archetypal picture of a symmetric headland on an otherwise straight coast generating a vortex pair either side of the headland with resultant offshore residual from the centre of the headland can be altered significantly by imbalances in tidal flow, asymmetries in geographical configuration and variations in the seabed. Pingree (1978) first suggested that the formation of sandbanks near headlands could be caused by the tidal residual gyres around both sides of headlands, or 'tidal stirring'. One central argument was that if inertial forces are dominant then the gyres would be symmetric whereas if Coriolis effects were important asymmetry in the gyres was to be expected, favouring the formation of an anticlockwise gyre (in the northern hemisphere). The morphology of the nearshore bathymetry could also be important in generating tidal torque through vortex stretching. Pingree and Maddock (1980) further investigated the effects of Coriolis force and bottom friction on the generation of depth-averaged tidal residual currents and gyres around an island with sloping topography and found that a quadrupole was generated around the island, with the Coriolis effect creating stronger clockwise gyres. They also found that the advection of vorticity and vortex stretching tended to balance the curl of the mean bottom stress. Signell and Harris (1999) tested the "tidal stirring" hypothesis of asymmetric sandbank formation by using a computational model to simulate the sediment transport and morphological changes of the sea bed, and found that the influence of the Coriolis force on the formation of the sandbanks on both sides of a headland was insignificant. In computations with a depth-averaged model Yang and Wang (2013) found that around headlands with a shoaling seabed clockwise tidal residual gyres were generally stronger than the anticlockwise gyre because of the effect of Coriolis force. Indeed, Robinson (1983) and Ridderinkhof (1989) suggested that frictional torque and vortex stretching are the dominant mechanisms of introducing vorticity to the mean flow. This can be understood in a qualitative manner by considering that the depth-averaged effects of bottom friction will become proportionately larger in shallow water, thereby creating a stronger damping effect on depth-averaged currents. Quasi-shore parallel flows will therefore be preferentially damped on their shoreward side, introducing shear in the cross-shore velocity profile and hence creating vorticity. Also, as a flow moves up the bathymetry gradient into shallower water it will gain negative vorticity as the water columns are

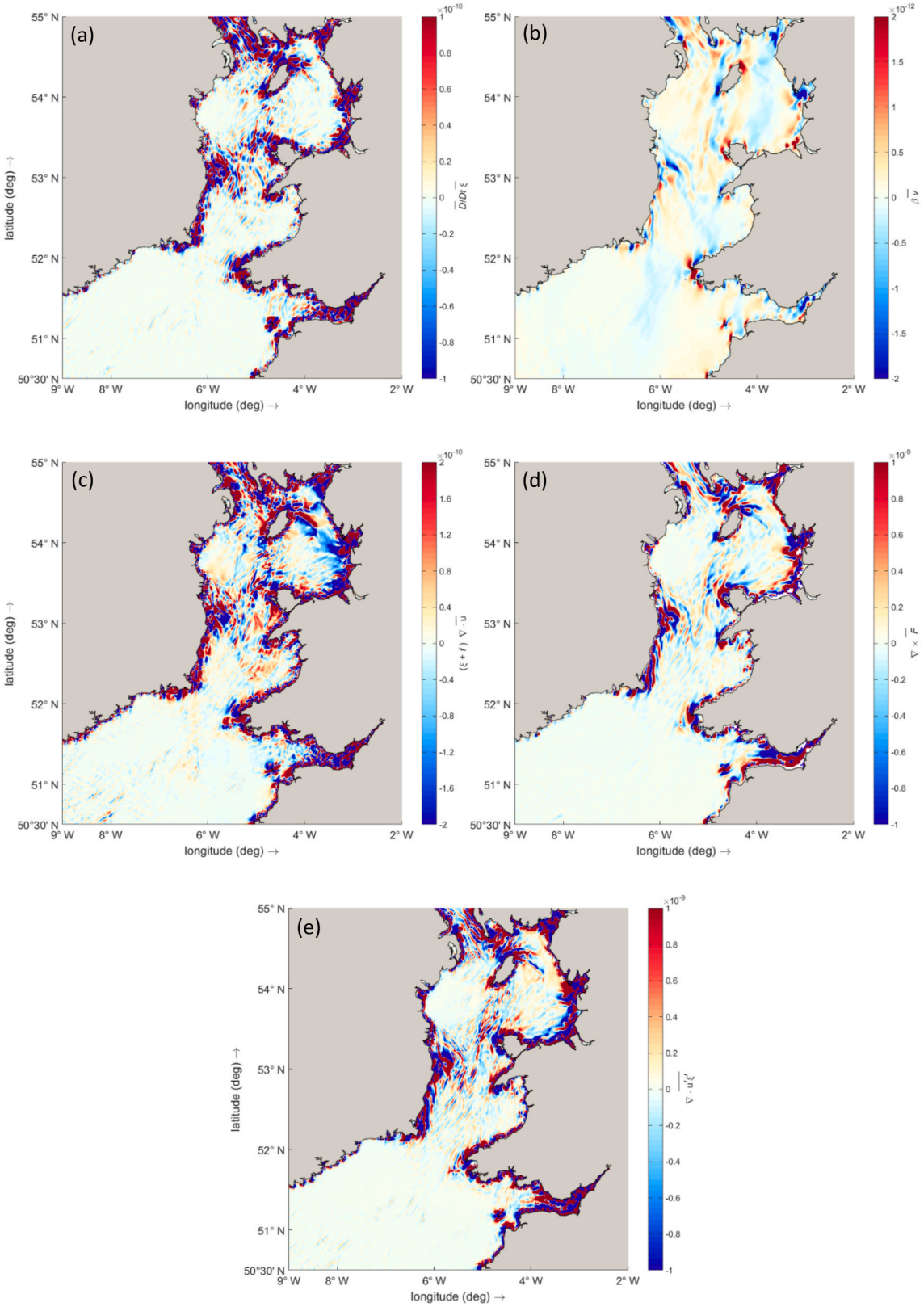

Fig. 10. Terms in the time averaged vorticity equation, (s^{-2}): (a) advection of absolute vorticity by the mean flow; (b) advection of planetary vorticity; (c) vorticity generation by stretching by the mean flow; (d) vorticity generation by bed friction; (e) eddy vorticity flux divergence. Note that the contour colour range varies between (a) to (e). (For interpretation of the references to colour in this figure legend, the reader is referred to the Web version of this article.)

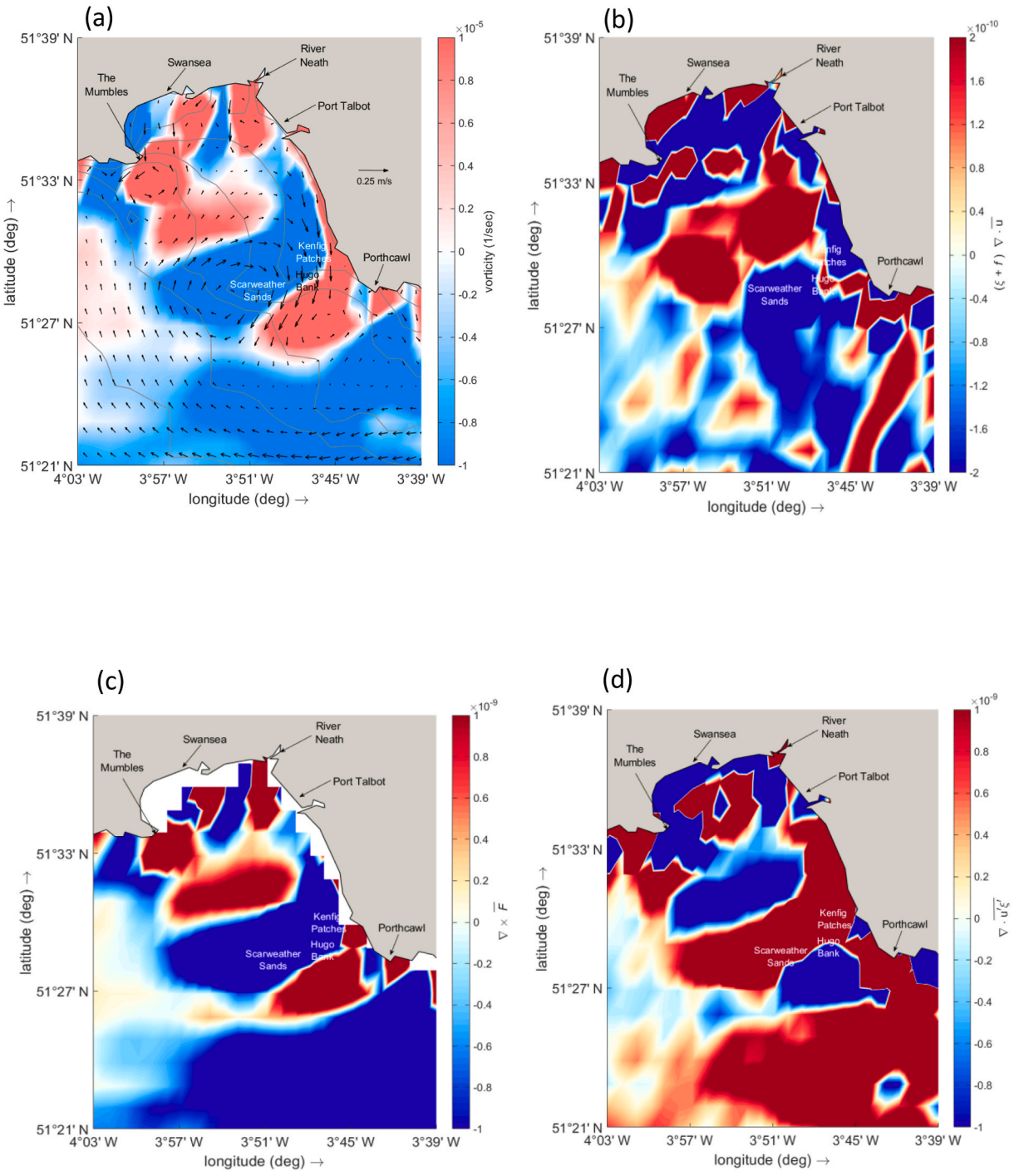

Fig. 11. Swansea Bay: (a) Computed residual currents, (ms^{-1}), and vorticity contours, (s^{-1}); (b) vortex stretching by the residual flow, (s^{-1}); (c) time mean bed friction term, (s^{-1}); (d) mean eddy vorticity flux divergence, (s^{-1}).

compressed, and flow into deeper water will gain positive vorticity as the water column is stretched.

In a depth-averaged hydrodynamic modelling study (Park and Wang, 2000) suggest that advection and stretching terms dominate the vorticity balance at headlands for large Rossby number flows (i.e. fast flows round small headlands). Further, they found asymmetry in the residual dipole with the anticlockwise gyre being stronger. In their idealised study of the influence of seabed slope and Coriolis force on sandbank formation near headlands Jones et al. (2006) found that the Coriolis force does not play an important role in sandbank generation associated with headlands, particularly where the nearshore slope is large in which vortex stretching is dominant. Neill et al. (2007) concluded that accounting for secondary flow effects can enhance the formation of a sand bank at the centre of a cyclonic headland-generated gyre compared to simple depth-averaged models. Berthot and Pattiaratchi (2006) demonstrated, using a 3-D model, that complex three-dimensional circulation patterns arising from interactions between tidal currents and topographic features could influence the distribution of sediments.

Indeed, inferring sediment transport and accretion solely from depth-averaged residual currents is not foolproof as it takes no account of many factors important for sediment transport such as: the

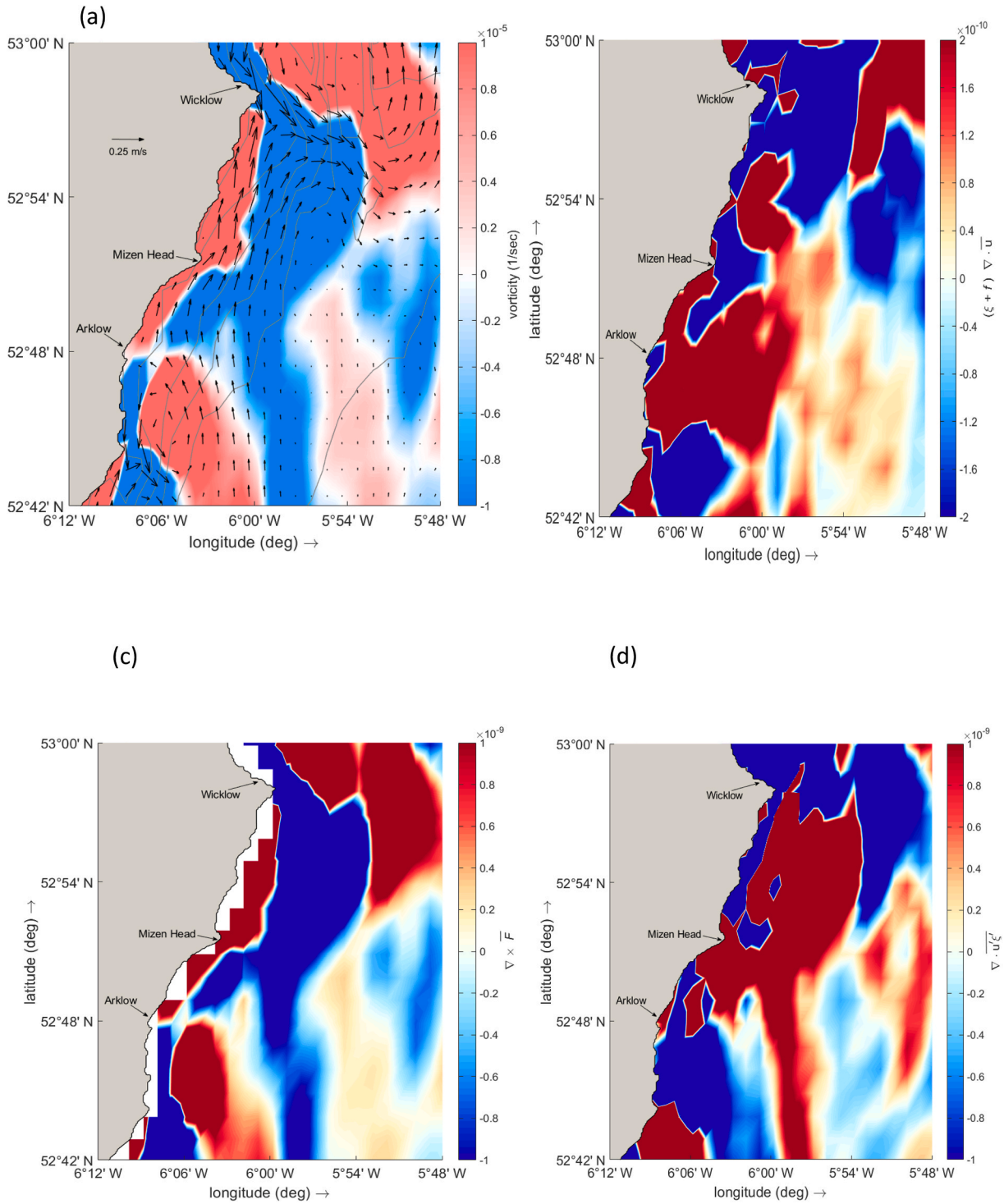

Fig. 12. Arklow Sand/Wicklow: (a) Computed residual currents, (ms^{-1}), and vorticity contours, (s^{-1}); (b) vortex stretching by the residual flow, (s^{-1}); (c) time mean bed friction term, (s^{-1}); (d) mean eddy vorticity flux divergence, (s^{-1}).

availability of sediments; a threshold of movement required for transport to take place; the composition and size of sediments; resuspension of sediments by non-tidal processes such as waves and surges; three dimensional effects and secondary flows.

From our three study sites we have found cases that both agree and disagree with many of the conclusions drawn from studies of simplified coastal bathymetries. From dynamical considerations the variable depth of the nearshore bathymetry is clearly important in vorticity production and destruction, as is the nonlinear advection of vorticity. However, we find that the primary balance is between the frictional torque and the eddy vorticity flux divergence. Thus, the constraints on the flow imposed by irregular topography and bathymetry must also be important in real-life situations. The narrowing and widening of channels, the shoaling and deepening of the seabed, cause local acceleration and deceleration of the instantaneous tidal flow introducing enhanced frictional effects and velocity shear. This leads to distortion of the tidal oscillations and consequent generation of vorticity through the tidal stresses. Expanding the eddy vorticity flux divergence:

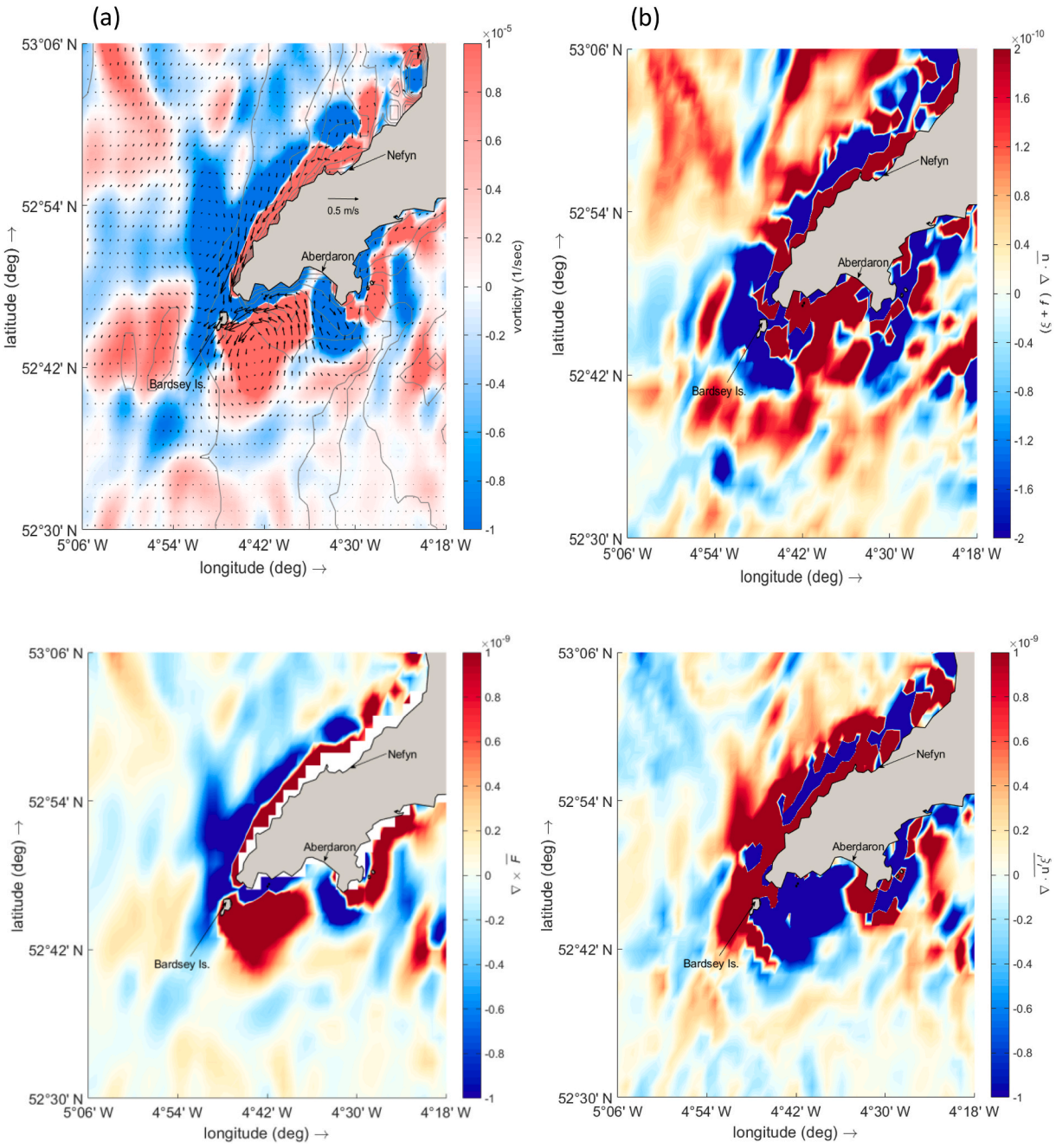

Fig. 13. Llŷn Peninsula: (a) Computed residual currents, (ms^{-1}), and vorticity contours, (s^{-1}); (b) vortex stretching by the residual flow, (s^{-1}); (c) time mean bed friction term, (s^{-1}); (d) mean eddy vorticity flux divergence, (s^{-1}).

$$\nabla.\overline{\mathbf{u}'\xi'} = \overline{\mathbf{u}'.\nabla\xi'} + \overline{\xi'\nabla.\mathbf{u}'} \tag{13b}$$

it is clear that this contains the time averaged contributions from both advection of vorticity and vortex stretching by the tidal oscillations.

6. Conclusions

We have investigated the mechanisms driving tidal residual currents computed over a period of one year using a high resolution computational model covering the Irish and Celtic Seas. This area has a strongly varying bathymetry, highly irregular coastline and extremely energetic tides. We have provided theoretical justification, through consideration of the vorticity dynamics, that the anisotropy of tidal oscillations is a crucial factor in the genesis of residual currents. Time series of depth-averaged velocities and surface elevations have been used to calculate time series of derived quantities allowing an analysis of terms in the time average vorticity equation.

Our main findings are:

- Tidal stresses can be written in the form of the divergence of a vorticity flux in the tidally averaged vorticity equation;
- This flux divergence can be linked to the anisotropy of the tidal eddies where they are approximately horizontally non-divergent;
- Assuming horizontal non-divergence a measure of anisotropy may be calculated, in a straightforward manner from the eddy velocity tensor, which has strong similarities to the tidal ellipses of the major tidal harmonic;

- From our simulations the time mean vorticity balance is dominated by the frictional torque and the eddy vorticity flux divergence. Vorticity advection and vortex stretching by the residual flow are of secondary importance in the vorticity balance;
- The anisotropy of the tidal eddies is a crucial ingredient in the vorticity balance and the forcing of tidal residual currents.

The type of modelling procedure described here could be tailored to derive tidal residual currents over springs and neaps which could be of use for ecological applications, and the DELFT modelling suite has capability to include the effects of prescribed wind fields and wave conditions. The effect of each element, and their combination, on residual currents could thereby be determined.

Given the prominence of the frictional torque in the regional vorticity balance of the residual flow, some further consideration of the detailed formulation of bed shear stress term in the momentum equations may be due. For turbulent flows the shear stress exerted by the fluid on the bed is generally asserted to be of quadratic form with respect to the mean current, and is widely used in tidal studies (e.g. Prandle, 2009). This form was questioned by Reid (1957) who suggested modifications when surface wind was present and more recently by Yang et al. (2015) who suggested modifications for smooth bare and vegetated channels.

CRediT authorship contribution statement

D.E. Reeve: Writing – review & editing, Writing – original draft, Project administration, Methodology, Funding acquisition, Conceptualization. **J.M. Horrillo-Caraballo:** Writing – original draft, Visualization, Software, Methodology. **H. Karunarathna:** Writing – review & editing.

Declaration of competing interest

The authors declare that they have no known competing financial interests or personal relationships that could have appeared to influence the work reported in this paper.

Data availability

Data will be made available on request.

Acknowledgements

The authors gratefully acknowledge funding from the European Regional Development Fund through the Welsh Government via the SEACAMS2 project, as well as discussions with Prof Ian Masters and Dr Iain Fairley.

Appendix A. Governing equations

Here, we provide an outline of the derivation of the Reynolds' averaged, depth-averaged governing equations and derivation of the vorticity equation. We start with the assumption of incompressible flow and integrate from the spatially varying sea bed depth below mean sea level, h, to the free surface height, η, relative to its equilibrium position. The components of velocity in the x- and y-directions are u and v respectively. We also write $H = h + \eta$ as the total water depth. The depth averaged continuity equation may be written as:

$$\frac{\partial \eta}{\partial t} + \frac{\partial (H\widetilde{u})}{\partial x} + \frac{\partial (H\widetilde{v})}{\partial y} = 0 \tag{A1}$$

where a tilde denotes a depth average quantity and deviations from the depth average quantity will be denoted by a caret, ˆ. We further assume that the density is constant, that atmospheric pressure is constant and that motions are hydrostatic.

The Reynolds' averaged momentum equation in the x-direction may be written as:

$$\frac{\partial [u]}{\partial t} + [u]\frac{\partial [u]}{\partial x} + [v]\frac{\partial [u]}{\partial y} - f[v] = -g\frac{\partial [\eta]}{\partial x} - \left[\frac{1}{\rho}\left(\frac{\partial \tau_{xx}}{\partial x} + \frac{\partial \tau_{yx}}{\partial y} + \frac{\partial \tau_{zx}}{\partial z}\right)\right] \tag{A2}$$

where g is the acceleration due to the Earth's gravity, f is the Coriolis parameter, ρ is the density of sea water, x and y are local Cartesian coordinates, t is time, $H(x,y)$ is the total water depth and $\tau_{..}$ are the components of stress arising from viscous stresses and turbulent Reynolds' stresses. Square brackets denote averaging over the turbulent time scale and deviations from this average are denoted by an asterisk. The stress terms are usually considered the sum of viscous stress representing the averaged effect of molecular motions, and turbulent Reynolds' stresses representing the averaged effect of momentum transfer due to turbulent fluctuations. So, for example:

$$\tau_{xx} = \mu\frac{\partial [u]}{\partial x} - \rho[u^{*}u^{*}] \tag{A3}$$

A suitable value of viscosity coefficient μ has to be assigned and a turbulence closure model used to determine the velocity correlation term. Integrating A2 over depth, and applying a stress balance at the sea bed, and taking the applied surface stress to be zero allows the last term on the righthand side of A2 to be expressed in terms of a bed stress where

$$\tau_{bx} = -\left(\tau_{xx}\frac{\partial(-h)}{\partial x} + \tau_{xy}\frac{\partial(-h)}{\partial y} - \tau_{zx}\right) \tag{A4}$$

Substituting A4 into A2 and integrating over depth yields

$$\frac{\partial \widetilde{u}}{\partial t} + \widetilde{u}\frac{\partial \widetilde{u}}{\partial x} + \widetilde{v}\frac{\partial \widetilde{u}}{\partial y} - f\widetilde{v} = -g\frac{\partial \eta}{\partial x} + \frac{1}{H}\frac{\partial}{\partial x}\int_{-h}^{\eta}\left(\frac{\tau_{xx}}{\rho} - \widehat{u}^{2}\right)dz + \frac{1}{H}\frac{\partial}{\partial y}\int_{-h}^{\eta}\left(\frac{\tau_{yx}}{\rho} - \widehat{u}\widehat{v}\right)dz - \frac{1}{H}\frac{\tau_{bx}}{\rho} \tag{A5}$$

and similarly for the y-direction. The depth-averaged, Reynolds' averaged shallow water equations are collectively Equation (A1), together with Equation (A5) and its equivalent for the y-direction.

The velocity correlation terms involving deviations from the depth average represent spreading of momentum over the water column. These terms also require parameterising in terms of the averaged variables in order to close the system of equations. One simple closure model is to combine the effects of the different stresses into a single dispersion mechanism:

$$\int_{-h}^{\eta}\left(\frac{\tau_{xx}}{\rho}-\widehat{u}^2\right)dz=E_{xx}\frac{\partial(H\widetilde{u})}{\partial x}\int_{-h}^{\eta}\left(\frac{\tau_{yy}}{\rho}-\widehat{v}^2\right)dz=E_{yy}\frac{\partial(H\widetilde{v})}{\partial y}\int_{-h}^{\eta}\left(\frac{\tau_{yx}}{\rho}-\widehat{u}\widehat{v}\right)dz=E_{xy}\left(\frac{\partial(H\widetilde{u})}{\partial y}+\frac{\partial(H\widetilde{v})}{\partial x}\right) \tag{A6}$$

where E_{xx}, E_{yy} and E_{xy} are eddy dispersion coefficients which have to be assigned a suitable value. The bottom shear stress is commonly written as a quadratic function of depth and Reynolds' averaged velocity (U, V):

$$\underline{\tau_b}=\left(c_f U\sqrt{U^2+V^2}, c_f U\sqrt{U^2+V^2}\right) \tag{A7}$$

where c_f is a friction coefficient with a typical value of 0.0025, (see Prandle, 2009). The closure model A6 is one of several options offered in the DELFT suite. In our simulations the eddy dispersion coefficients were set to zero.

The equation for the vertical component of vorticity of the depth-averaged flow is found by forming

The 'horizontal curl' of A5 and its equivalent for the y-direction:

$$\frac{\partial\xi}{\partial t}+U\frac{\partial\xi}{\partial x}+V\frac{\partial\xi}{\partial y}+(\xi+f)\left(\frac{\partial U}{\partial x}+\frac{\partial V}{\partial y}\right)+\beta V=-\frac{1}{\rho}\left(\frac{\partial}{\partial x}\left(\frac{\tau_{by}}{H}\right)-\frac{\partial}{\partial y}\left(\frac{\tau_{bx}}{H}\right)\right) \tag{A8}$$

where $\xi = \partial V/\partial x$ - $\partial U/\partial y$, $\delta = \partial U/\partial x + \partial V/\partial y$, $\beta = df/dy$, which is equivalent to Equation (3).

Appendix B. Derivation of tidally-averaged equations

The depth-averaged momentum and vorticity equations are:

$$\frac{D\mathbf{u}}{Dt}+f\mathbf{k}x\mathbf{u}+g\nabla\eta=\mathbf{F} \tag{B1}$$

$$\frac{D\zeta}{Dt}+\zeta\nabla.\mathbf{u}=\mathbf{k}.\nabla x\mathbf{F} \tag{B2}$$

We write $\boldsymbol{F}$, $\boldsymbol{u}$, ζ and η as the sum of a tidally averaged component, denoted by an overbar, and an eddy component that fluctuates from this average, denoted by a prime. Thus Eq. (B1) becomes:

$$\frac{\partial(\overline{\mathbf{u}}+\mathbf{u}')}{\partial t}+(\overline{\mathbf{u}}+\mathbf{u}').\nabla(\overline{\mathbf{u}}+\mathbf{u}')+f\,\mathbf{k}x(\overline{\mathbf{u}}+\mathbf{u}')+\nabla(\overline{\eta}+\eta')=\mathbf{F}+\mathbf{F}' \tag{B3}$$

Applying a time average to Eq. (B3), with the assumption that the time average of primed variables are zero and the mean surface excursion from equilibrium is zero yields:

$$\overline{\frac{\partial(\overline{\mathbf{u}}+\mathbf{u}')}{\partial t}}+\overline{\overline{\mathbf{u}}.\nabla\overline{\mathbf{u}}}+\overline{\overline{\mathbf{u}}.\nabla\mathbf{u}'}+\overline{\mathbf{u}'.\nabla\overline{\mathbf{u}}}+\overline{\mathbf{u}'.\nabla\mathbf{u}'}+f\overline{\mathbf{k}x\overline{\mathbf{u}}}=\overline{\mathbf{F}} \tag{B4}$$

Simplifying, and using the fact that the time average of a time averaged quantity is identical to the time average,

$$\overline{\mathbf{u}}.\nabla\overline{\mathbf{u}}+\overline{\mathbf{u}'.\nabla\mathbf{u}'}+f\mathbf{k}x\overline{\mathbf{u}}=\overline{\mathbf{F}} \tag{B5}$$

Similarly, applying a time average to the vorticity equation, (Eq. B2), yields

$$\overline{\mathbf{u}}.\nabla\overline{\zeta}+\overline{\zeta}\nabla.\overline{\mathbf{u}}+\overline{\mathbf{u}'.\nabla\zeta'}+\beta\overline{v}+\overline{\zeta'\nabla.\mathbf{u}'}=\mathbf{k}.\nabla x\overline{\mathbf{F}} \tag{B6}$$

where $\beta = df/dy$ and v is the meridional component of $\boldsymbol{u}$. an overbar denotes a time average and a prime denotes a temporal fluctuation. The absolute vorticity, ζ, is the sum of the relative vorticity, ξ, and the planetary vorticity, f, due to the rotation of the Earth. Eq. (B6) may be written in terms of the relative vorticity as

$$\overline{\mathbf{u}}.\nabla\overline{\xi}+(\overline{\xi}+f)\nabla.\overline{\mathbf{u}}+\beta\overline{v}=\mathbf{k}.\nabla x\overline{\mathbf{F}}-\overline{\nabla.\mathbf{u}'\xi'} \tag{B7}$$

where the terms involving the eddy vorticity have been combined together.

Appendix C. Analysis of the depth-averaged velocity correlation tensor

The depth-integrated velocity correlation tensor, $\mathbf{C}$, may be written as the sum of an isotropic and anisotropic (trace-free) parts:

$$\boldsymbol{C}=\begin{pmatrix}\overline{u'^2} & \overline{u'v'}\\ \overline{u'v'} & \overline{v'^2}\end{pmatrix}=\begin{pmatrix}K & 0\\ 0 & K\end{pmatrix}+\begin{pmatrix}M & N\\ N & -M\end{pmatrix} \tag{C1}$$

If the tidal eddies are approximately horizontally non-divergent the velocity may be written in the form of a streamfunction $\psi = a\cos(kx^* - \omega_1 t)\cos(ly^* - \omega_2 t)$, which corresponds to an elliptical tidal eddy flow, such that it has wave number k and l along local x and y axes x^* and y^* oriented along the major and minor axes. In this case the local value of M will be proportional to $l^2 - k^2$ as long as the averaging period averages over the phases of the velocity components. In this case the quantity $\alpha = \sqrt{(M^2+N^2)}/K$ simplifies to $(l^2-k^2)/(l^2+k^2)$ as shown by Hoskins et al. (1983). For the extreme case of purely rectilinear flow along the x-axis, l becomes infinite and α tends to 1. Similarly, for pure rectilinear flow in the y-axis (with x* running parallel to the y-axis) α tends to 1.

References

Amante, C., Eakins, B.W., 2009. ETOPO1 1 Arc-Minute Global Relief Model: Procedures, Data Sources and Analysis. NOAA Technical Memorandum NESDIS NGDC-24. National Geophysical Data Center, NOAA. https://doi.org/10.7289/V5C8276M [June 2017].

Aubrey, D.G., Speer, P.E., 1985. A study of non-linear tidal propagation in shallow inlet/estuarine systems, Part I: Observations. Estuar. Coast Shelf Sci. 21, 185–205.

Berthot, A., Pattiaratchi, C., 2006. Mechanisms for the formation of headland-associated linear sandbanks. Continent. Shelf Res. 26 (8), p987–1004.

Bowden, K.F., 1980. Physical and dynamical oceanography of the Irish sea. In: Banner, F. T., Collins, M.B., Massie, K.S. (Eds.), The North-West European Shelf Seas: the Sea Bed and the Sea in Motion II. Physical and Chemical Oceanography, and Physical Resources, Elsevier Oceanography Series, vol. 24. Elsevier Scientific Publishing Company, Amsterdam, pp. 391–413. Part B.

Bracewell, R., 1999. The Filtering or Interpolating Function, Sinc(x). The Fourier Transform and its Applications, third ed. McGraw-Hill, New York, pp. 62–64.

Chatzirodou, A., Karunarathna, H., Reeve, D.E., 2017. Modelling 3D hydrodynamics governing island-associated sandbanks in a proposed tidal stream energy site. Appl. Ocean Res. 66, 79–94.

De Swart, H.E., Zimmerman, J.T.F., 2009. Morphodynamics of tidal inlet systems. Annu. Rev. Fluid Mech. 41, 203–229.

Dronkers, J., 1986. Tidal asymmetry and estuarine morphology. Neth. J. Sea Res. 20 (2/3), 107–131.

Egbert, G.D., Erofeeva, S.Y., 2002. Efficient inverse modeling of barotropic ocean tides. J. Atmos. Ocean. Technol. 19 (2), 183–204.

EMODnet Bathymetry Consortium – EMODNET, 2016. EMODnet Digital Bathymetry (DTM). http://doi.org/10.12770/c7b53704-999d-4721-b1a3-04ec60c87238. October 2016.

Friedrichs, C.T., Aubrey, D.G., 1988. Non-linear tidal distortion in shallow well-mixed estuaries: a synthesis, Estuarine. Coast Shelf Sci. 27, 521–545.

Gallo, M.N., Vinzon, S.B., 2005. Generation of overtides and compound tides in Amazon estuary. Ocean Dynam. 55, 441–448.

Garrett, C., Greenberg, D., 1977. Predicting changes in tidal regime: the open boundary problem. J. Phys. Oceanogr. 7, 171–181. https://doi.org/10.1175/1520-0485(1977)007<0171:PCITRT>2.0.CO;2.

Guo, L.C., Wang, Z.B., Townend, I.H., He, Q., 2019. Quantification of tidal asymmetry and its nonstationary variations. JGR: Oceans 124, 773–787.

Haltiner, G.J., Williams, R.T., 1980. Numerical Prediction and Dynamic Meteorology, second ed. Wiley, New York, p. 496.

Heathershaw, A.D., Hammond, F.D.C., 1979. Tidal currents: observed tidal and residual circulations and their response to meteorological conditions. Swansea Bay (SKER) Project Topic 4, I.O.S. Report No. 92. https://eprints.soton.ac.uk/14375/1/14375-01.pdf (accessed 25/04/22).

Holt, J.T., James, I.D., 2006. An assessment of the fine-scale eddies in a high-resolution model of the shelf seas west of Great Britain. Ocean Model. 13, p271–291.

Horrillo-Caraballo, J.M., Reeve, D.E., 2008. Morphodynamic behaviour of a nearshore sandbank system: the Great Yarmouth Sandbanks, U.K. Mar. Geol. 254 (1–2), 91–106. https://doi.org/10.1016/j.margeo.2008.05.014.

Horrillo-Caraballo, J.M., Yin, Y., Fairley, I., Karunarathna, H., Masters, I., Reeve, D.E., 2021. A comprehensive study of the tides around the Welsh coastal waters. Estuar. Coast Shelf Sci. 254, 107326 https://doi.org/10.1016/j.ecss.2021.107326.

Hoskins, B.J., James, I.N., White, G.H., 1983. The shape, propagation and mean-flow interaction of large-scale weather systems. J. Atmos. Sci. 40, p1595–1612.

Howarth, M.J., 2005. Hydrography of the Irish Sea. SEA6 Technical Report. UK Department of Trade and Industry's offshore energy - Strategic Environmental Assessment programme, p. 30.

Hulscher, J.M.H., de Swart, H.E., de Vriend, H.J., 1993. The generation of offshore tidal sand banks and sandwaves. Continent. Shelf Res. 13 (11), p1183–1204.

Huthnance, J.M., 1973. Tidal current asymmetries over the norfolk sandbanks. Estuar. Coast Mar. Sci. 1, 89–99.

Jones, O.P., Simons, R.R., Jones, E.J.W., Harris, J.M., 2006. Influence of seabed slope and Coriolis effects on the development of sandbanks near headlands. J. Geophys. Res. 111 (C3).

Lesser, G.R., Roelvink, J.A., van Kester, J.A.T.M., Stelling, G.S., 2004. Development and validation of a three-dimensional morphological model. Coast. Eng. 51 (8–9), 883–915.

McCave, I.N., 1970. Sand waves in the north sea off the coast of holland. Mar. Geol. 10, p199–225.

Moore, R.D., Wolf, J., Souza, A.J., Flint, S.S., 2009. Morphological evolution of the dee estuary, eastern Irish sea, UK: a tidal asymmetry approach. Geomorphology 103, 588–596. https://doi.org/10.1016/j.geomorph.2008.08.003.

Müller, P., 2006. The Equations of Oceanic Motions. CUP, Cambridge, UK, p. 291.

Neill, S.P., Hashemi, M.R., Elliot, A.J., 2007. An enhanced depth-averaged tidal model for morphological studies in the presence of rotary currents. Continent. Shelf Res. 27, p82–102.

Neill, S.P., Hashemi, R., Lewis, M.J., et al., 2014. The role of tidal asymmetry in characterizing the tidal energy resource of Orkney. Renew. Energy 68, 337–350.

Nihoul, J.C.J., Ronday, F.C., 1975. The influence of tidal stress on the residual circulation. Tellus 29, p484–490.

Olbert, A.I., Dabrowski, T., Nash, S., Hartnett, M., 2012. Regional modelling of the 21st century climate changes in the Irish Sea. Continent. Shelf Res. 41, p48–60.

Owen, A., 1980. The tidal regime of the Bristol Channel: a numerical modelling approach. Geophys. J. Roy. Astron. Soc. 62, p59–75.

Park, M.-J., Wang, D.-P., 2000. Tidal vorticity around a coastal promontory. J. Oceanogr. 56, p261–273.

Parker, B.B., 2007. Tidal Analysis and Prediction. NOAA Special Publication NOS CO-OPS 3, vol. 378. NOAA NOS Center for Operational Oceanographic Products and Services, Silver Spring, MD, USA. https://doi.org/10.25607/OBP-191.

Pingree, R.D., 1978. The formation of the Shambles and other banks by tidal stirring of the seas. J. Mar. Biol. Assoc. U. K. 58, p211–226 (in anticlockwise gyre reinforce f, -> enhance sandbank?).

Pingree, R.D., Maddock, L., 1979. The tidal physics of headland flows and offshore tidal bank formation. Mar. Geol. 32, 269–289.

Pingree, R.D., Maddock, L., 1980. Tidally induced residual flows around an island due to both frictional and rotational effects, geophys. J. R. Astr. Soc. 63, p533–546.

Pingree, R.D., 1980. Physical oceanography of the Celtic Sea and English channel. Part B. In: Banner, F.T., Collins, M.B., Massie, K.S. (Eds.), The North-West European Shelf Seas: the Sea Bed and the Sea in Motion II. Physical and Chemical Oceanography, and Physical Resources. Elsevier Oceanography Series, vol. 24. Elsevier Scientific Publishing Company, Amsterdam, pp. 415–465, 0422-9894.

Prandle, D., 1978. Residual flows and elevations in the southern North Sea. Proc. Roy. Soc. Lond. A 359 (1697), 187–228.

Prandle, D., 1984. A modelling study of the mixing of 137Cs in the seas of the European continental shelf. Phil. Trans. Roy. Soc. Lond. 310, 407–436.

Prandle, D., Ryder, D.K., 1989. Comparison of observed (HF radar) and modelled nearshore velocities. Continent. Shelf Res. 9 (11), p941–963.

Prandle, D., 2009. Estuaries: Dynamics, Mixing, Sedimentation and Morphology. CUP, UK, p. 236.

Pugh, D.T., 1996. Tides, Surges and Mean Sea-Level (Reprinted with Corrections). John Wiley & Sons, Ltd., Chichester, UK, p. 486.

Reid, O., 1957. Modification of the Quadratic Bottom-Stress Law for Turbulent Channel Flow in the Presence of Surface Wind-Stress, TECHNICAL MEMORANDUM NO.93. BEACH EROSION BOARD CORPS OF ENGINEERS.

Ridderinkhof, H., 1989. Tidal and residual flows in the western Dutch wadden sea III: vorticity balances. Neth. J. Sea Res. 24 (1), 9–26.

Robinson, I.S., 1979. The tidal dynamics of the Irish and Celtic Seas. Geophys. J. Int. 56 (1), 159–197. https://doi.org/10.1111/j.1365-246X.1979.tb04774.x.

Robinson, I.S., 1983. Tidally induced residual flows. In: Johns, B. (Ed.), Physical Oceanography of Coastal and Shelf Seas. Elsevier, Amsterdam, pp. 321–356.

Sanay, R., Voulgaris, G., Warner, J.C., 2007. Tidal asymmetry and residual circulation over linear sandbanks and their implication on sediment transport: a process-oriented numerical study. J. Geophys. Res. 112. C12015.

Signell, R.P., Harris, C.K., 1999. Modeling sand-bank formation around a tidal headland. In: Spaulding, M.L., Butler, H.L. (Eds.), Estuarine and Coastal Modeling; Proceedings of the Sixth International Conference. American Society of Civil Engineers, Reston, pp. 209–222.

Simonsen, A.J., Krogstad, P., 2005. Turbulent stress invariant analysis: clarification of existing terminology. Phys. Fluids 17, 088103.

Takasugi, Y., Fujiwara, T., Sugimoto, T., 1994. Formation of sand banks due to tidal vortices around straits. J. Oceanogr. 50 (1), 81–98. https://doi.org/10.1007/BF02233858.

Uncles, R.J., 1982. Computed and observed residual currents in the Bristol Channel. Oceanol. Acta 5 (1), p11–20.

Van Ormondt, M., Nederhoff, K., Van Dongeren, A., 2020. Delft Dashboard: a quick set-up tool for hydrodynamic models. J. Hydroinf. 22 (3), p510–527.

Weatherall, P., Marks, K.M., Jakobsson, M., Schmitt, T., Tani, S., Arndt, J.E., Rovere, M., Chayes, D., Ferrini, V., Wigley, R., 2015. A new digital bathymetric model of the world's oceans. Earth Space Sci. 2 (8), 331–345. https://doi.org/10.1002/2015EA000107.

Williams, R.G., Wilson, C., Hughes, C.W., 2007. Ocean and atmosphere storm tracks: the role of eddy vorticity forcing. J. Phys. Oceanogr. 37, p2267–2289.

Yang, J.Q., Kerger, F., Nepf, H.M., 2015. Estimation of the bed shear stress in vegetated and bare channels with smooth beds. Water Resour. Res. 51, 3647–3663. https://doi.org/10.1002/2014WR016042.

Yang, Z., Wang, T., 2013. Tidal residual eddies and their effect on water exchange in Puget Sound. Ocean Dynam. 65, 995–1009. https://doi.org/10.1007/s10236-013-0635-z.

Zimmerman, J.T.F., 1978. Topographic generation of residual circulation by oscillatory tidal currents. Geophys. Astrophys. Fluid Dynam. 11, 35–47.

Zimmerman, J.T.F., 1981. Dynamics, diffusion and geomorphological significance of tidal residual eddies. Nature 290, 549–555.